Frequency Tunable First-Overtone and Fundamental Band CO Laser System:

parametric study, gain kinetics and model development for highly excited vibrational transitions of CO molecule

Final Report on Contract **SPC-99-4018**

February 1999 - December 1999

P.N.Lebedev Physics Institute, Moscow, Russia	*Troitsk Institute for Innovation and Fusion Research, Troitsk, Moscow Region, Russia*	*Institute of High Temperature, Moscow, Russia*
Principal Investigator, Scientific Leader: Prof. A. Ionin	**Scientific leader:** Prof. A. Napartovich	**Scientific leader:** Prof. Yu. Konev
Investigetors: Mr. A. Kotkov	**Investigetors:** Dr. A. Kurnosov	
Mr. L. Seleznev	Mr. N. Turkin	
Mr. D. Sinitsyn		
Mr. Yu. Klimachev		

Moscow 1999

REPORT DOCUMENTATION PAGE

Form Approved OMB No. 0704-0188

1. AGENCY USE ONLY (Leave blank)	2. REPORT DATE	3. REPORT TYPE AND DATES COVERED
	1999	Final Report

4. TITLE AND SUBTITLE

Frequency Tunable First Overtone And Fundamental Band CO Laser System: Parametric Study, Gain Kinetics, And Model Development For Highly Excited Vibrational Transitions Of CO Molecule

5. FUNDING NUMBERS

F61775-99-WE018

6. AUTHOR(S)

Dr. Andre Ionine

7. PERFORMING ORGANIZATION NAME(S) AND ADDRESS(ES)

Lebedev Physics Institute
53 Leninsky Prospect
Moscow 117924
Russia

8. PERFORMING ORGANIZATION REPORT NUMBER

N/A

9. SPONSORING/MONITORING AGENCY NAME(S) AND ADDRESS(ES)

EOARD
PSC 802 BOX 14
FPO 09499-0200

10. SPONSORING/MONITORING AGENCY REPORT NUMBER

SPC 99-4018

11. SUPPLEMENTARY NOTES

12a. DISTRIBUTION/AVAILABILITY STATEMENT

Approved for public release; distribution is unlimited.

12b. DISTRIBUTION CODE

A

13. ABSTRACT (Maximum 200 words)

This report results from a contract taskingLebedev Physics Institute as follows: The contractor will investigate physical processes in highly excited vibrational transitions (V of 20 to 40) of the CO molecule for use in frequency-selective first overtone and fundamental band CO lasers to include, but not be limited to, small signal gain and saturated gain kinetics.

14. SUBJECT TERMS

EOARD, Gas Discharge, gas lasers, Carbon monoxide lasers, Overtone CO lasers

15. NUMBER OF PAGES

63

16. PRICE CODE

N/A

17. SECURITY CLASSIFICATION OF REPORT	18. SECURITY CLASSIFICATION OF THIS PAGE	19. SECURITY CLASSIFICATION OF ABSTRACT	20. LIMITATION OF ABSTRACT
UNCLASSIFIED	UNCLASSIFIED	UNCLASSIFIED	UL

CONTENTS

Introduction

A detailed experimental and theoretical study of first-overtone (FO) CO laser using both intracavity spectral filter (Ionin et al., 1997a, 1998a, b) and dielectric output couplers (Ionin et al., 1998c, 1999a, b, Basov et al., 1999a, b, c) demonstrated, that pulsed multiline FO CO laser can operate within spectral range of 2.5 - 4.1 μm and its output efficiency can come up to 20%, in principle. Output efficiency of 11% was observed in the experiments with multiline FO CO laser using some output couplers from AF Research Lab (Ionin et al., 1999a), theoretical prognosis for the laser with the same output couplers but with suppressed fundamental band (FB) lasing being 17%. A feasibility of pulsed FO CO laser frequency tuning was demonstrated in (Ionin et al., 1999a) for the first time. However, single-line FO CO laser efficiency ~0.2% obtained in the first experiments was not high enough. Therefore, one of the objectives of the Project was to study output characteristics of FO CO laser using other combinations of dielectric output couplers from AFRL with paying much more attention to spectral features of multiline spectrum. The second objective of the Project was to study single-line FO CO laser with different gratings for an achievement of maximum output efficiency and frequency broad band tunability of single-line FO CO laser, multiquantum theory suggested in (Ionin et al., 1998e, 1999d) being taken into consideration for theoretical description of the laser.

The third objective of the Project, which could be considered as a feasibility study, was to measure experimentally and describe theoretically small signal gain (SSG) and saturated gain on selected FO transitions using both threshold characteristics of FO CO laser and pulsed single-line free-running FO CO laser master-oscillator-power amplifier (MOPA) laser system. The results obtained are supposed to be used for a description of vibrational kinetics of highly excited vibrational levels of CO molecule.

The fourth objective of the Project was an extension of the theoretical model for a description of plasma characteristics of radio-frequency (RF) discharge carbon monoxide laser.

The final report consists of four parts. Part 1 describes multiline FO CO laser using dielectric mirrors. Part 2 concerns frequency tunable single-line FO CO laser. MOPA carbon monoxide system is discussed in Part 3. Part 4 describes modeling plasma characteristics in RF discharge CO laser.

1. Multiline pulsed FO CO laser with dielectric couplers

1.1. Alternation of vibrational band intensities in multiline pulsed first-overtone CO laser spectrum

1.1.1. Introduction

First-overtone (FO) CO laser, which operates on two-quantum vibrational transitions V+2→V [Bergman et al., 1997, Basov et al., 1978], has very rich ro-vibrational spectrum lying within spectral range from 2.5 up to 4.2 μm [Gromoll-Bohle et al., 1989, Bachem et al., 1993, Basov et al., 1999a,b,c, Ionin et al., 1999a,b] and corresponding to vibrational transitions from 6→4 up to 38→36. The laser has high output efficiency up to 11% in pulsed mode of operation [Basov et al., 1999a,b,c]. There was noted in the theoretical paper [Suchkov et al., 1979], that there should be an alternation of vibrational band intensities, i.e. an alternation of strong and weak vibrational bands, in pulsed free-running FO CO laser spectrum. The "spectrum alternation" is determined by two sets of cascade transitions operating independently, which can happen, if the rate of radiative transitions is much higher than that of vibrational-vibrational exchange. Up to now this effect has not been observed experimentally, because much more attention has seemed to be paid to spectrum wavelengths, but not to the intensity (energy) distribution over vibrational bands [Basov et al., 1978, 1980, 1999a,b,c, Ionin et al., 1998a,b, 1999a,b].

The effect of "spectrum alternation" or "zebra-like" spectrum of pulsed FO CO laser, which was observed experimentally for the first time, is discussed in the paper. The influence of laser mixture composition and gas density on the "zebra-like" spectrum is also discussed.

1.1.2. Experimental facility

The experimental facility was described earlier in [Basov et al., 1999a,b,c, Ionin et al., 1998a,b,c, 1999a,b]. Cryogenically cooled pulsed e-beam controlled discharge laser was used with active length of 1.2 m. The pump pulse length was 25 μs, and specific input energy (SIE) changed from ~50 up to ~700 J/l Amagat. Laser mixture $CO:N_2:He$ with different content of nitrogen and helium at the temperature ~100 K and density from 0.02 up to 0.3 Amagat were used.

The 2.2 m laser resonator consisted of spherical dielectric mirror with radius of curvature of 10.0 m and flat dielectric mirror situated on the laser chamber [Basov et al., 1999a,b,c]. The active laser volume determined by mirror size and intracavity diaphragms was 0.85 l. The effective reflectivity $R=(R_1R_2)^{1/2}$ for the equivalent laser resonator consisted of the two mirrors with the reflectivities R_1 and R_2 is presented in Fig. 1.1a. Spectral characteristics of the laser mirrors (reflectance and transmittance) were studied with a PERKIN-ELMER 9836 spectrophotometer. FO

CO laser spectrum was measured by a home-made grating (150 grooves/mm) spectrometer. In comparison with papers [Basov et al., 1999a,b,c, Ionin et al., 1998a,b, 1999b], where rather rough visual estimation of vibrational band energy was done by using IR video-camera, in this paper the spectral distribution of FO CO laser was thoroughly measured by a thermocouple calorimeter or by computer processing of video-image of the laser spectrum located in the spectrometer focal plane.

1.1.3. Experimental and theoretical results

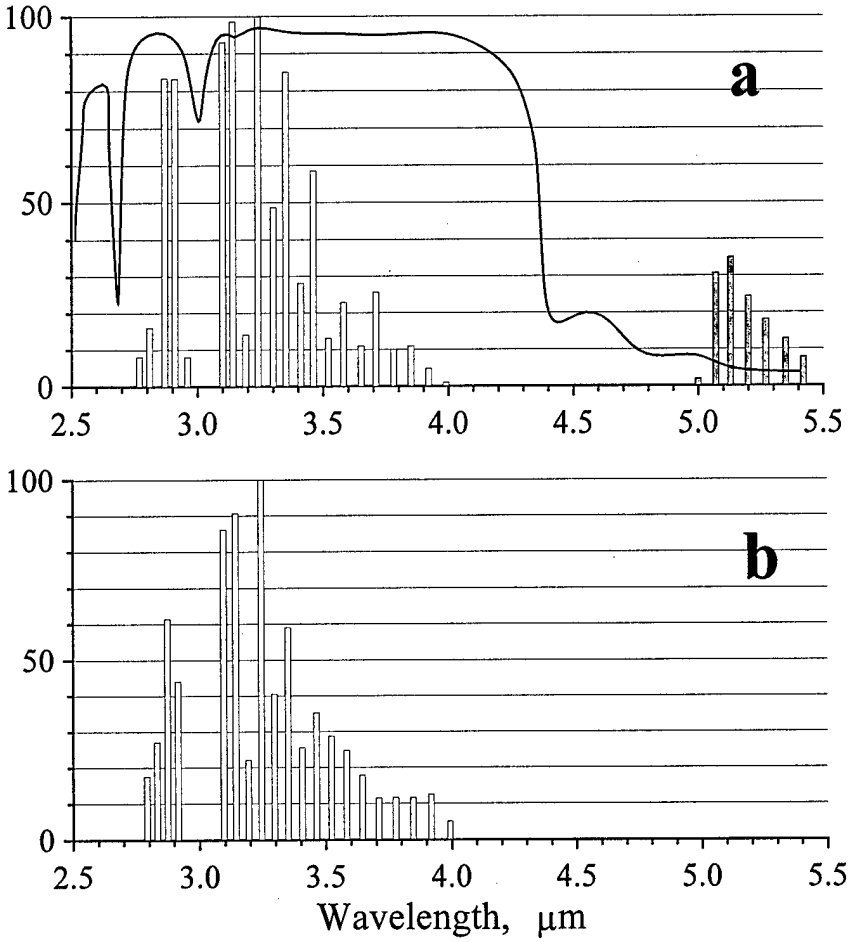

Fig. 1.1. Effective reflectivity of output couplers and output laser spectra.
a - experiment; b - theory
$CO:N_2:He=1:9:10$; N=0.12 Amagat; SIE=300 J/l Amagat; T=100 K

The experimentally measured spectral distribution of the CO laser energy over the vibrational bands is presented in Fig. 1.1a. Gas mixture $CO:N_2:He=1:9:10$ at density 0.12 Amagat was used. An alternation of FO CO laser output energy over vibrational bands ("zebra-like" spectrum) is clearly seen from the figure. There was no such effect for fundamental band (FB) lasing near 5 μm (Fig. 1.1a). Fig. 1.1b presents the theoretically calculated spectral distribution for the experimental conditions. This also indicates an intensity alternation. The observed effect, as was mention above, is connected with two sets of cascade transitions operating independently. There is a good correlation between the experimental and theoretical spectral distribution for the FO CO laser

spectrum. The output energy of FB lasing was very low [Basov et al., 1999a,b,c], with the theory predicting no FB lasing.

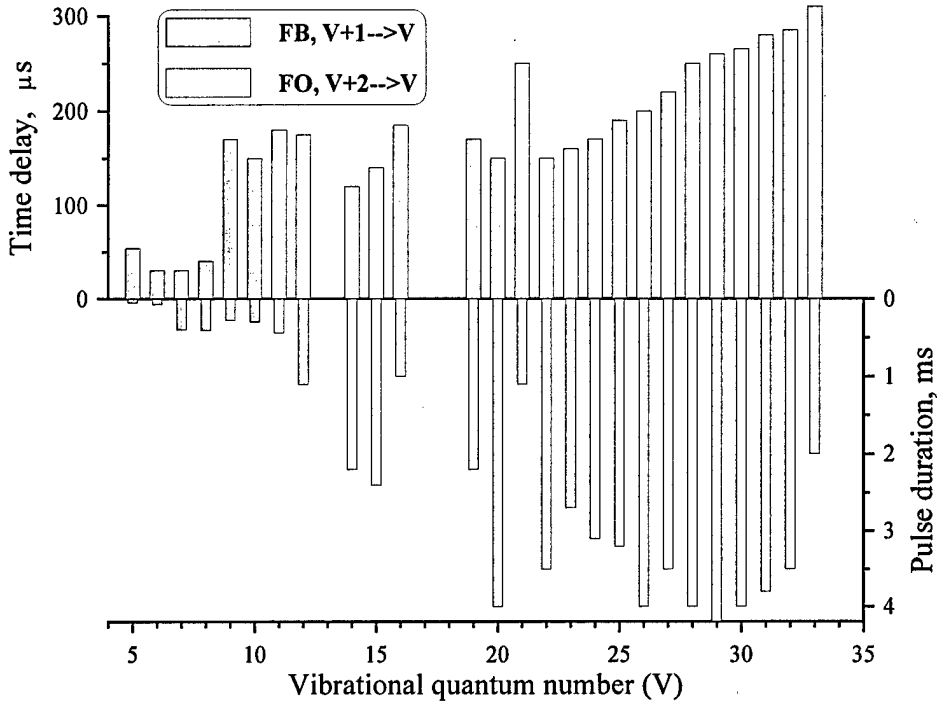

Fig. 1.2. Time delay and pulse duration vs vibrational quantum number of lower laser level for the same experimental conditions as in Fig. 1.

Time characteristics (pulse duration and time delay) measured by Ge:Au photodetector for each vibrational transition corresponding to Fig. 1.1 are presented in Fig. 1.2 for both FO and FB lasing. Time delay was determined as a time interval between pump and laser pulse beginnings. FB lasing took place on vibrational transitions lower than those of FO CO laser. FB CO laser pulse length and time delay (0.05-0.5 ms and 30-60 μs, respectively) were shorter than those of FO CO laser (1.0-4.0 ms and 130-500 μs, respectively). FO CO lasing time delay increased monotonously for vibrational numbers from V=22 up to V=33. Time delays ~150-180 μs for two vibrational transitions with V=9, 10 of fundamental band were much longer than for other FB transitions and comparable with those of two nearest FO transitions with V=11, 12. The effect seems to demonstrate how FO lasing on higher vibrational transitions (V=11, 12) correlates with FB lasing on lower transitions (V=9, 10) because of cascade mechanism of inversion population formation.

Although, the "spectrum alternation" was claimed in [Suchkov et al., 1979] to take place only in nitrogen containing laser mixtures, the effect was observed for various gas mixtures ($CO:N_2$=1:9, CO:He=1:4 and pure CO) (Fig. 1.3a-c). Two sets of vibrational bands corresponding to two different lasing cascades are designated by gray and black bars. "Zebra-like" spectrum was also detected near lasing threshold, when only a few (more than 4) vibrational bands were observed.

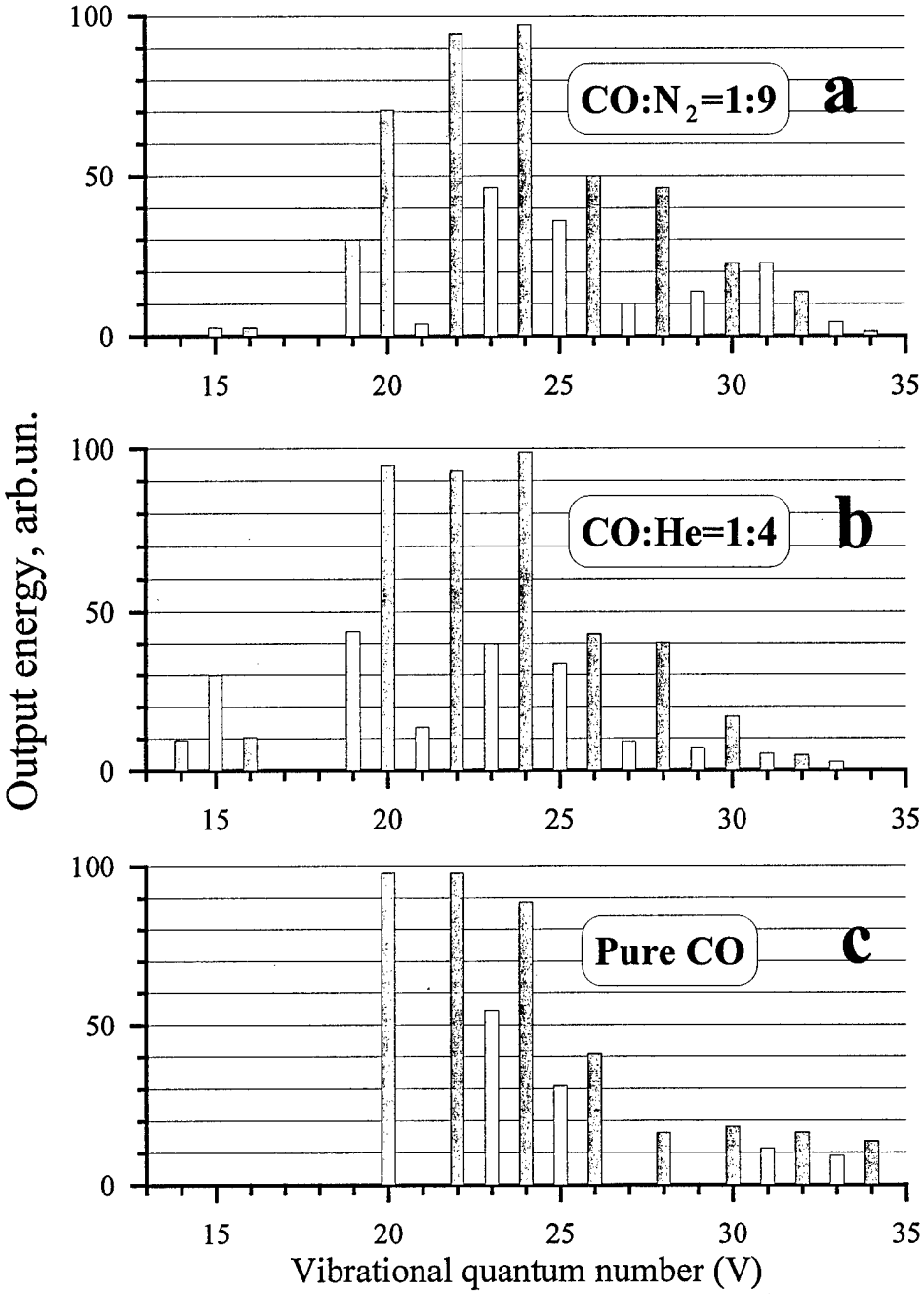

Fig. 1.3. "Zebra-like" spectra for FO CO laser operating on various laser mixtures CO:N_2=1:9 (a), CO:He=1:4 (b) and pure CO (c). N=0.12 Amagat, T=100 K

The "spectrum alternation" was observed for different gas density varying within 0.02 - 0.3 Amagat (Fig. 1.4a-d). An attempt of estimation of "spectrum alternation" visibility was undertaken, the visibility being defined as $V=(Q_{even}-Q_{odd})/(Q_{even}+Q_{odd})$ ratio (where Q_{even} (Q_{odd}) - total energy radiating through even (odd) cascade. Output energies on vibrational transitions from 22→20 up to 35→33 were taken into account only, because the spectral distribution over vibrational band for lower and higher transition had irregular behavior. "Spectrum alternation" visibility is presented in Fig. 1.5. The observed maximal visibility up to 0.6 corresponds to N=0.12 Amagat, the visibility V rapidly decreasing with gas density rise and fall.

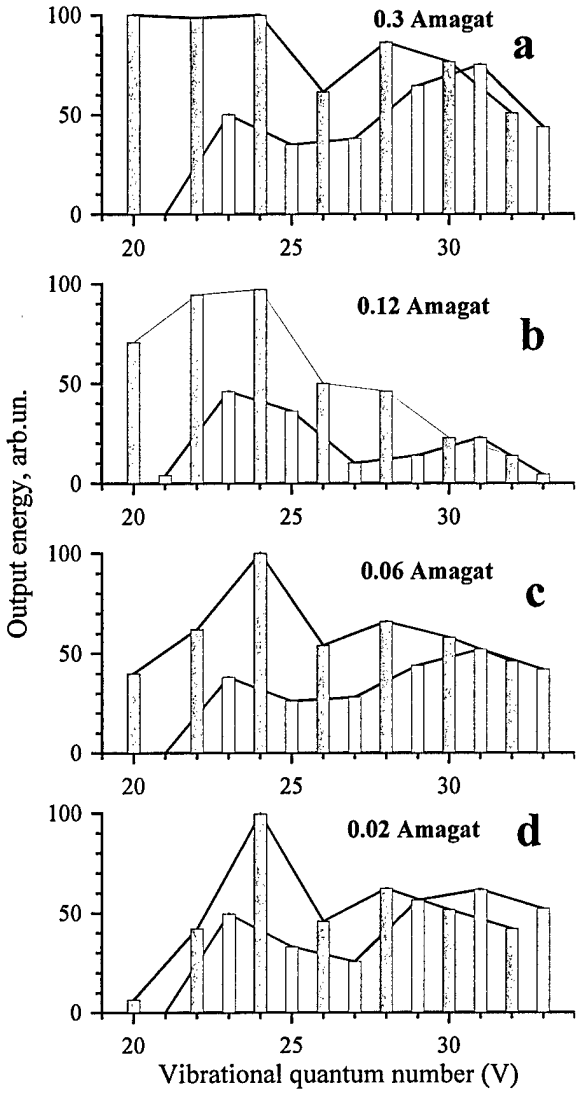

Fig. 1.4. "Zebra-like" spectra for FO CO laser operating at various gas densities 0.3 (a), 0.12 (b), 0.06 (c) and 0.02 (d) Amagat. CO:N_2=1:9, N=0.12 Amagat. The envelopes demonstrate two different cascades

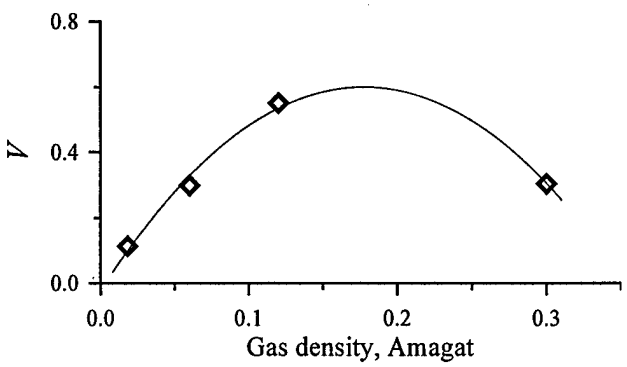

Fig. 1.5. "Spectrum alternation" visibility V vs. gas density. CO:N_2=1:9; T=100 K

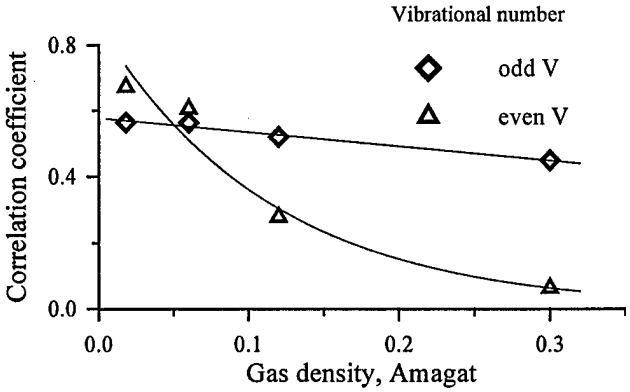

Fig. 1.6. Correlation coefficient for two sets of cascade vibrational transitions (odd and even) and effective reflectivity for the equivalent laser resonator for the same experimental conditions as in Fig. 3.

For the same experimental conditions, an empirical correlation coefficient [Bronshtein et al., 1986] corresponding to the spectral distributions of the two (odd and even) cascade sets (Fig. 1.4) and the effective reflectivity of the equivalent laser resonator (Fig. 1.1a) was obtained (Fig. 1.6) for various gas densities. It can be easily seen that both cascades well correlate with spectral reflectivity of the equivalent laser resonator, indicating lower small signal gain for both cascades at lower densities (~0.02-0.05 Amagat). For higher density strong even cascade does not correlate with the reflectivity curve, as compared with weak odd cascade, which testifies higher gain exceeding over threshold gain for the stronger cascade.

1.1.4. Conclusions

The alternation of pulsed FO CO laser output energy over vibrational bands (i.e. alternation of strong and weak vibrational bands over multiline FO CO laser spectrum) was experimentally observed for the first time. The alternation is connected with two sets of cascade vibrational transitions operating independently for the given experimental conditions. There is a good correlation between the experimental and theoretical FO CO laser spectrum. The influence of FO CO lasing on higher vibrational transitions upon FB CO lasing on lower vibrational transitions due to cascade mechanism of inversion population formation was demonstrated. The "spectrum alternation" was observed for different laser mixtures ($CO:N_2:He$; $CO:N_2$; CO:He and pure CO) for various gas density within interval of 0.02-0.3 Amagat and different SIE down to one close to the threshold condition. The effect is important for better understanding of kinetic processes taking place on highly excited vibrational levels of CO molecule.

1.2. Energetic and spectral characteristics of FO CO laser using different combinations of output couplers

Various combinations of dielectric couplers, which were not used in previous researches, were used for the FO CO laser.

FO CO laser output spectra for optical resonators consisting of M99+M99 and M98+M99 mirror sets are presented in Fig.1.7-10. The spectra were observed by IR video-camera and processed with a computer. FB lasing took place as well, but spectral measurements for this spectral region were not carried out. Fig.1.7 and Fig.1.9 demonstrate the output spectra for gas mixture $CO:N_2:He=1:9:10$. Fig.1.8 and Fig.1.10 demonstrate the output spectra for pure CO. The effect of spectrum alternation was weaker with M99+M99 mirror set as compared to M98+M99 set and stronger when using pure CO as active medium of FO CO laser for the fixed mirror set.

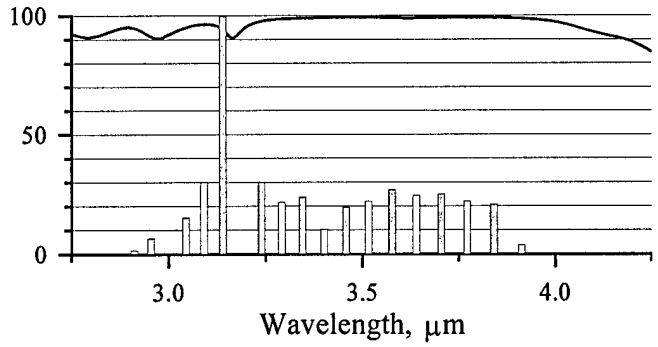

Fig.1.7. Effective reflectivity for M99+M99 mirror set and output spectrum of FO CO laser using the mirror set

$CO:N_2:He=1:9:10$; SIE=150 J/l Amagat N=0.12 Amagat

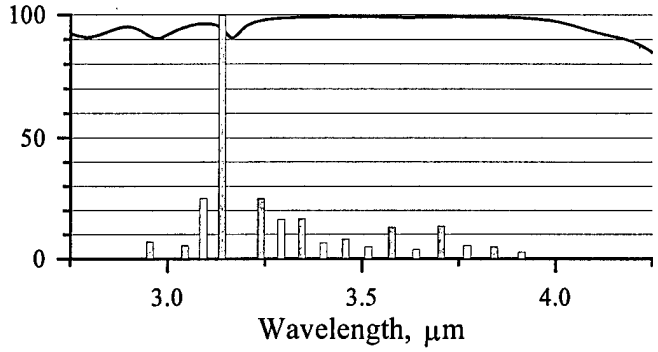

Fig.1.8. Effective reflectivity for M99+M99 mirror set and output spectrum of FO CO laser using the mirror set.

Pure CO;
SIE=360 J/l Amagat
N=0.12 Amagat

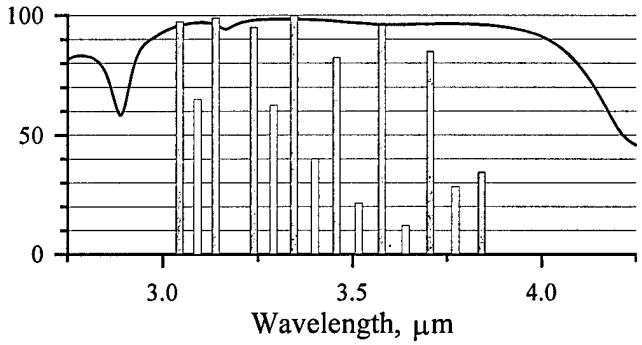

Fig.1.9. Effective reflectivity for M98+M99 mirror set and output spectrum of FO CO laser using the mirror set

$CO:N_2:He=1:9:10$;
SIE = 150 J/l Amagat
N=0.12 Amagat

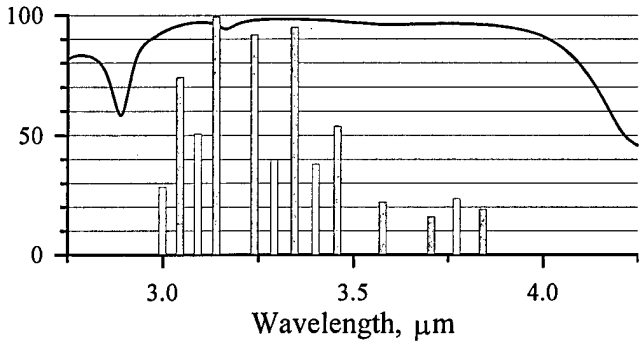

Fig.1.10. Effective reflectivity for M98+M99 mirror set and output spectrum of FO CO laser using the mirror set

Pure CO;
SIE = 360 J/l Amagat
N=0.12 Amagat

Output energy was measured for the FO CO laser using M99+M99 and M98+M99 mirror sets (as for M92+M99 set, see [Ionin et al., 1999a, Basov et al., 1999a,b,c]). The dependencies of output efficiency on specific input energy (SIE) are presented in Fig.1.11. Because of high effective reflectivity, which was close to ~100%, and strong FB lasing FO CO laser efficiency was much lower than 11% obtained for FO CO laser with M98+M98 mirror set and ~8% with M92+M99 set [Ionin et al., 1999a, Basov et al., 1999a,b,c], namely, less than 1.5% for the laser with M98+M99 set and less than 1% for M99+M99 set. When using pure CO as active medium, output efficiency was not higher than 0.3%. Therefore, for getting the highest FO CO laser efficiency, the best mirror set amongst all possible combinations of the mirrors delivered from the AFRL is M98+M98 mirror set [Ionin et al., 1999a, Basov et al., 1999a,b,c].

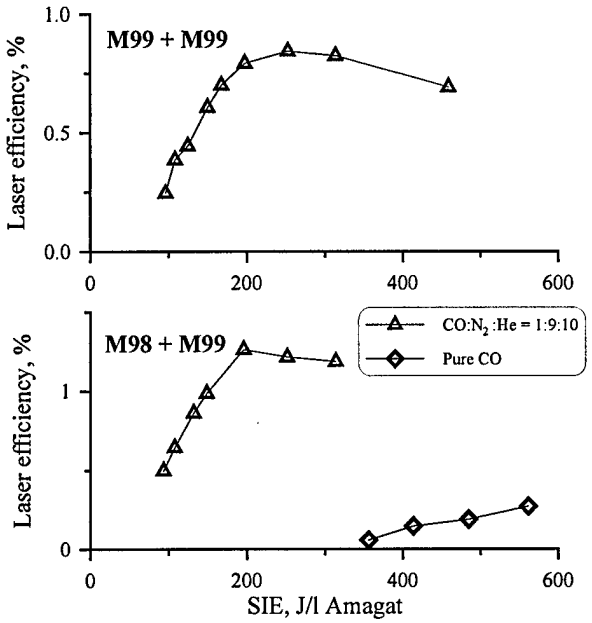

Fig.1.11. FO CO laser efficiency vs. specific input energy (SIE) for the laser with M99+M99 mirror set and M98+M99 set for gas mixture: $CO:N_2:He=1:9:10$ and pure CO.

1.3. Examination of mirrors' spectral characteristics

In the course of exploitation of mirrors from AFRL, some visually detectable changes in their surface turned into the discharge chamber appeared: a few point defects of size approximately 0.1-0.2 mm, and reflecting layer grew slightly turbid. Generally, both the laser radiation and X-ray emission from electron gun may act on mirror quality. To clear our their respective role and estimate how this action is important, two mirrors intensively exploited in the experiments were examined in respect of their spectral reflection and transmission variation: 1) A mirror with reflectance in overtone band 92-94% (M92); 2) A mirror with reflectance 98% (M98).

Methodology of measurements was the same as earlier described in the report (?). The only difference was in a number of mirror orientations relative to a spectral slit of the device: measurements were performed for four orientations and the result was calculated by averaging. In this way, the influence of point defects on the mirror surface on results was weakened. The measured characteristics were compared with correspondent characteristics of the mirrors taken before the exploitation was started.

A comparison of the measured data allows us to make the following conclusions:

1. Certainly, transmission of both mirrors in the range of CO overtone lasing ν=2400-4000 cm-1 increases. In average, transmission coefficient grows on 0.6% for the first mirror and on (0.4-0.5)% for the second mirror.
2. In the spectral range of the fundamental band ν=1600-2000 cm-1 transmission coefficient for both mirrors diminishes, decrement being 1-1.1% for the first mirror and 1.2-1.3% for the second one.

3. Examination of reflection properties showed that the reflection coefficient varies on approximately the same amount as the transmittance, however, in opposite direction. In particular, in the FO band reflection coefficient diminishes while in the FB it increases. It means that spectral selection of the FO lasing range for the mirrors under investigation became worse.
4. Value of total losses within mirrors associated with scattering and absorption in layers of the structure is of the order of error of measurements.

2. Frequency tunable single-line FO CO laser

2.1. Introduction

A carbon monoxide laser is a very attractive source of tunable mid-IR radiation for various applications. It can operate both in the fundamental band (FB) (V+1→V, λ~ 4.63 μm - 8.23 μm [Yardley, 1970, McCord et al., 1999]) and in the first-overtone (FO) [Bergman et al., 1977, Basov et al., 1978] (V+2→V, λ=2.5-4.2 μm [Basov et al., 1999a,b,c, Ionin et al., 1999a,b]) spectral range. The FO CO laser spectral range covers that of HF and DF lasers, with its ro-vibrational line spacings being several times less than that of those lasers. FO CO laser spectral lines coincide with a large number of absorption lines belonging to numerous organic and inorganic substances found in the atmosphere.

Previously, a single-line low pressure CW FO CO laser was developed which operated on 330 ro-vibrational lines and was frequency tuned within the spectral range of 2.6-4.1 μm [Gromoll-Bohle et al., 1989, Bachem et al., 1993]. This laser had a low output power of ~0.55 W and was used for spectroscopic applications [Murtz et al., 1998], which do not require high output power and output efficiency. Recently, we demonstrated a pulsed multiline FO CO laser that operated within 2.5-4.1 μm and had a maximum output efficiency up to 11%, with theoretical prognosis indicating obtainable laser efficiency up to 20% [Basov et al., 1999a,b,c, Ionin et al., 1999a]. This high output efficiency, combined with a spectral output energy of ~50 J/l Amagat, places the FO CO laser in the company of other high power lasers, such as CO_2, FB CO, HF and DF lasers. This also implies that it can be used for long distance atmospheric monitoring and for laser material processing (especially in the processing case where special selected wavelengths are needed [Ionin et al., 1996a, 1997b, 1998d]). Theoretical analysis of FO CO laser characteristics and their comparison with experimentally measured results may provide further progress in the study of energy transfer processes on highly excited vibrational levels of the CO molecule [Ionin et al., 1996b, 1998e, 1999c,d].

A frequency tunable pulsed FO CO laser is studied in this paper. The laser operates on more than 400 ro-vibrational lines corresponding to vibrational transitions from 12→10 up to 38→36 within spectral range 2.7-4.2 μm. Maximal single-line FO CO laser efficiency obtained experimentally comes up to 0.6%. The experimental data are compared with theoretical calculations.

2.2. Experimental conditions

The experiments were carried out on a cryogenically cooled e-beam controlled discharge laser with an active length of 1.2 m [Basov et al., 1999a,b,c, Ionin et al., 1999a,b]. The maximum e-beam current density was 20 mA/cm^2, with electron energy being 150 keV. The pump pulse length was 25 μs, and specific input energy (SIE) changed from ~50 up to ~700 J/l Amagat. The temperature of the gas mixture was 100 K.

The FO CO laser resonator consisted of a diffraction grating (G) operating in a Littrow configuration and a concave (r=10 m) copper mirror, the former being located at a distance of 0.4 m from a Brewster window made of CaF_2 and the latter being installed at the laser chamber. The polarization plane of intracavity radiation was perpendicular to the grating grooves (S-polarization). The laser resonator length was 2.5 m. There were two diaphragms inside the laser resonator. One with a diameter of 50 mm near the copper mirror, and another with a 30 mm diameter near the grating. The optical volume was 0.85 *l*. Normally, FO CO laser radiation was extracted through the zero diffraction order of the grating.

Three different diffraction gratings (G1 - G3) were used for spectral selection and tuning of FO CO laser radiation. According to the certificates, maximum efficiency for the first diffraction order of nonpolarized radiation took place at wavelengths λ_{max} =3.0 μm (G1), 2.7 μm (G2) and 3.2 μm (G3). The G1 and G3 gratings were made of Al coated glass and had 200 grooves per mm. The G2 grating was made of Au coated glass and had 420 grooves per mm. Output coupling of the gratings, defined as the ratio of output energy going through the zero diffraction order to the intracavity energy, was measured by a comparison of the output energy with that of the Fresnel reflection by an intracavity CaF_2 flat plate. The output coupling T is presented in Figs. 2.1c, 2.3b and 2.4c. Output energy was measured by a thermocouple calorimeter.

Wavelength tuning of the laser radiation was effected by rotation of the grating. Single-line lasing was checked by a homemade diffraction grating spectrometer using an IR video camera for detection of IR radiation. Theoretically calculated FO CO laser wavelengths corresponding to different ro-vibrational transitions were used for identification of experimentally observed FO CO laser spectral lines (**Table** 2.1).

2.3. Experimental results

Fig. 2.1a demonstrates single-line FO CO laser efficiency versus laser wavelength. When using grating G1, FO CO laser radiation was frequency tuned within the spectral range of 2.7 - 4.1 μm, corresponding to the overtone vibrational transitions from 12→10 up to 37→35. Maximum output efficiency was 0.085% for the wavelength 3.34 μm (ro-vibrational transition 28→26 P(11)).

A nitrogen free laser mixture (CO:He=1:4) was used at a gas density 0.12 Amagat (SIE was 320 J/l Amagat). It should be noted that single-line FO CO lasing was obtained on highly excited CO transitions with output coupling of ~ 30%; i.e., grating efficiency was not higher than 70%. This indicates that small signal gain on high overtone transitions of CO molecule is at least larger than ~ 0.2 m^{-1}.

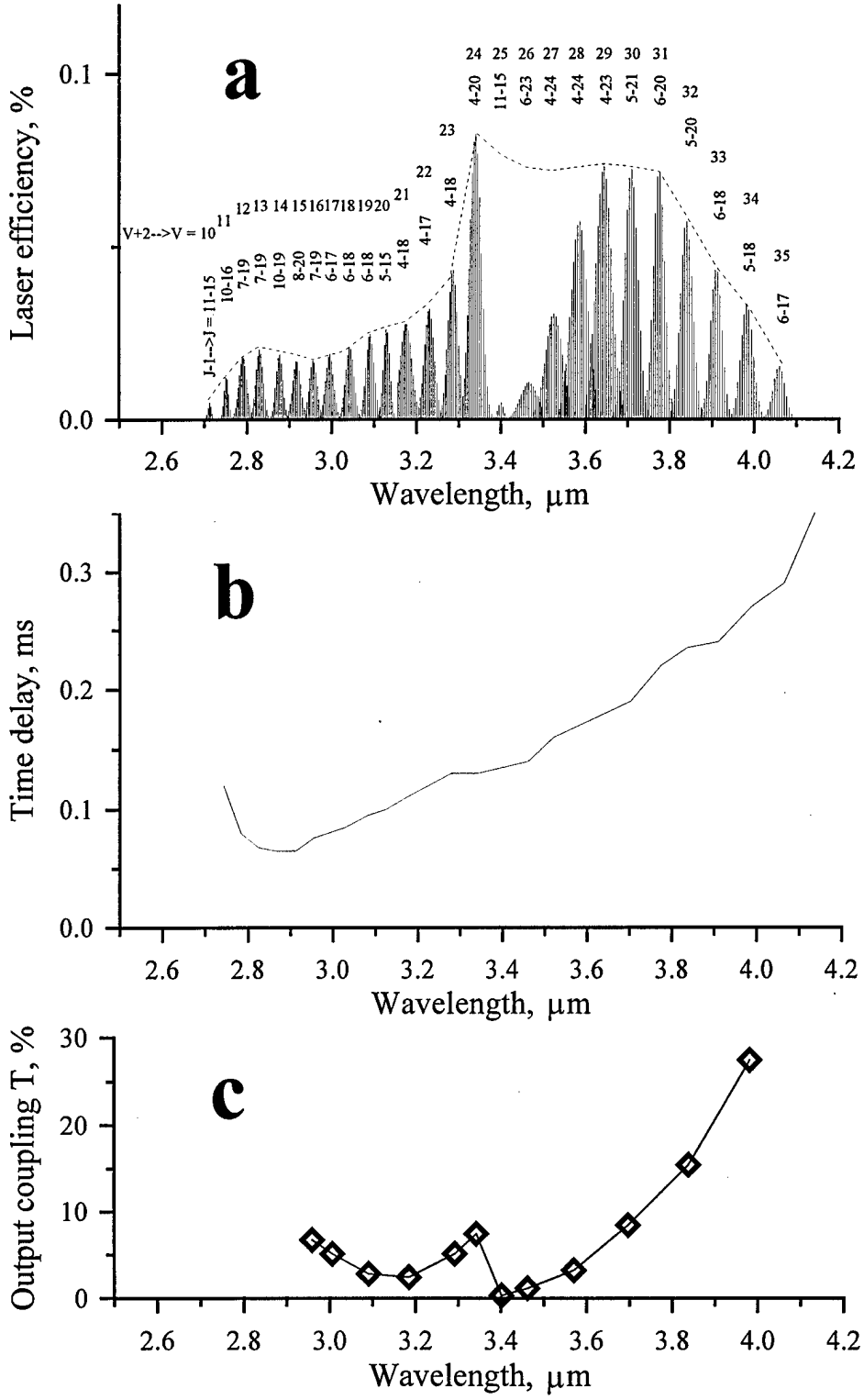

Fig. 2.1. Output laser efficiency (a), time delay of the laser pulse (b) and output coupling of diffraction grating G1 (c) vs. wavelength. Dotted line (a) is an envelope of maximum efficiency obtained with optimal laser cavity. CO:He=1:4; 0.12 Amagat; SIE=320 J/l Amagat.

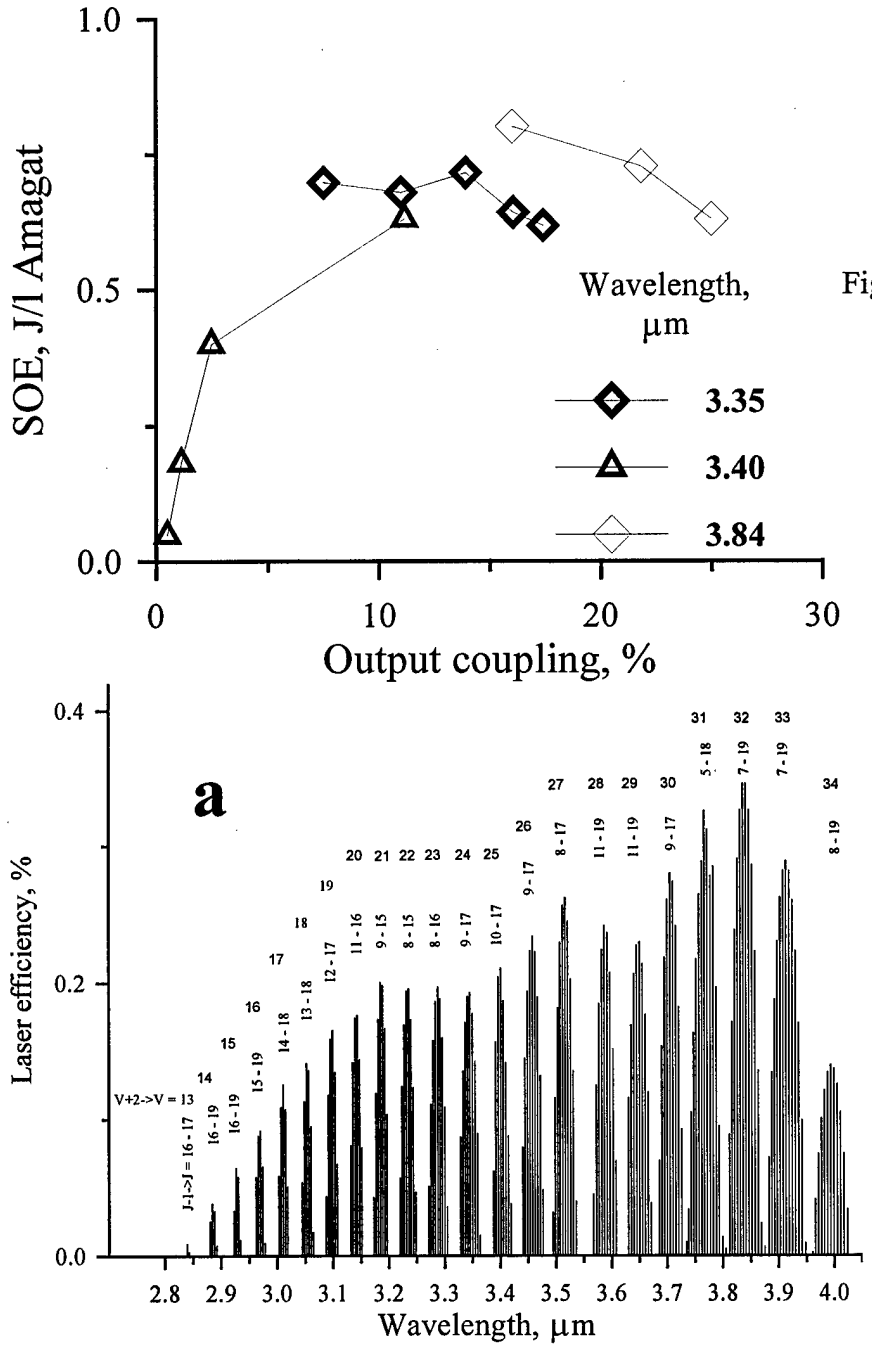

Fig.2.2. Specific output energy (SOE) vs. output coupling for three different wavelengths 3.35, 3.40 and 3.84, output coupling of diffraction grating G1 being 7.5, 0.5 and 16%, respectively. CO:N_2=1:9; 0.12 Amagat; SIE=350 J/l Amagat.

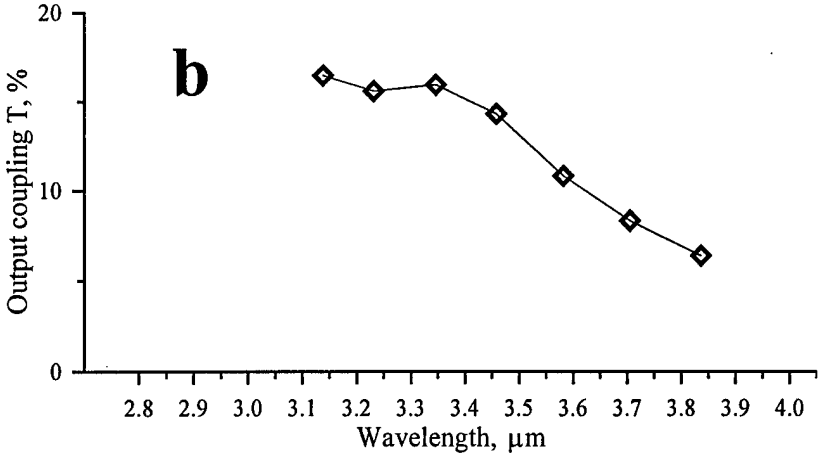

Fig. 2.3. Output laser efficiency (a) and output coupling of diffraction grating G2 (b) vs. wavelength. CO:N_2=1:9; 0.12 Amagat; SIE=360 J/l Amagat.

An anomaly in the spectral distribution (a spectral hole) near the wavelength 3.4 μm is connected with the spectral properties (Fig. 2.1c) of grating G1; namely, very low output coupling of ~ 0.5% (very high grating efficiency). Fig.2.2 demonstrates dependencies SOE on output coupling varied by using the Fresnel reflection of an intracavity CaF_2 flat plate for three different wavelengths 3.35, 3.40 and 3.84, output coupling of diffraction grating G1 being 7.5, 0.5 and 16%, respectively. An increase of the output coupling up to ~ 10% resulted in much higher output efficiency for 3.4 μm laser wavelengths corresponding to the "spectral hole". The dotted line in Fig. 2.1a represents an envelope of FO CO laser efficiency for optimized output coupling of the resonator with grating G1.

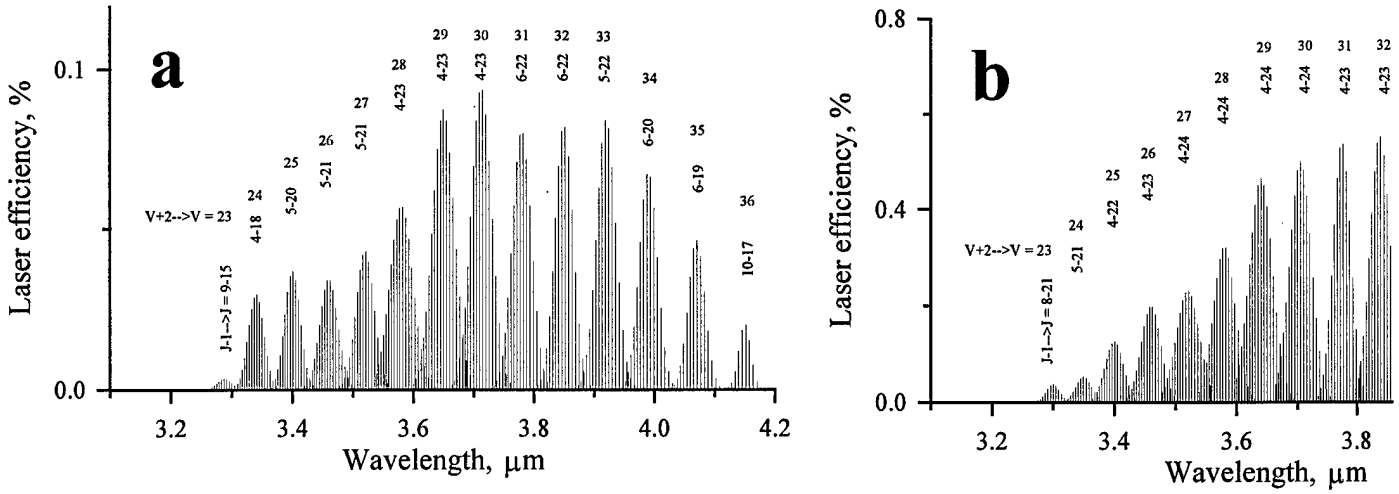

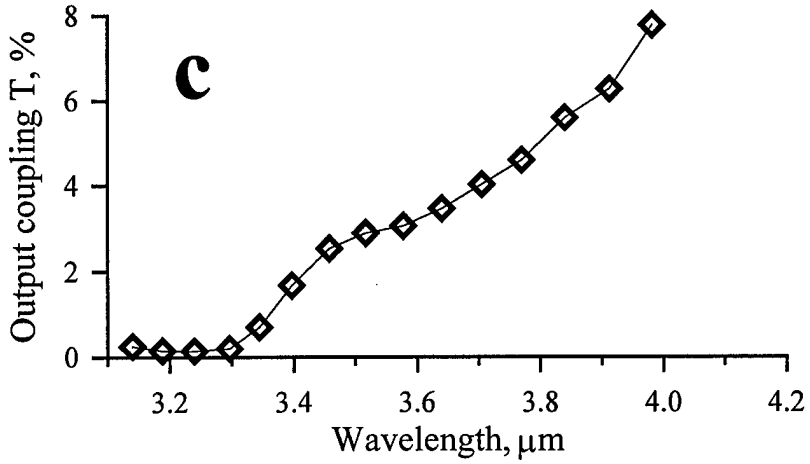

Fig. 2.4. Output laser efficiency for two different gas mixtures (a, b) and output coupling of diffraction grating G3 (c) vs. wavelength. Gas density=0.12 Amagat. CO:He=1:4, SIE = 320 J/l Amagat (a); $CO:N_2$=1:6, SIE = 500 J/l Amagat (b).

The single-line FO CO laser efficiency and output coupling for grating G2 are presented in Figs. 2.3a, b. A gas mixture with high nitrogen content ($CO:N_2$=1:9) at gas density 0.12 Amagat was used. SIE was 360 J/l Amagat. Using nitrogen in the laser mixture resulted in a SOE and output efficiency rise. Experimentally, the maximum SOE (1.24 J/l Amagat) and laser efficiency (0.34%) was obtained for ro-vibrational transitions 34→32 P(12) and P(13) at 3.83 μm.

Fig. 2.4 demonstrates FO CO laser efficiency versus wavelength for grating G3 when using gas mixtures of CO:He=1:4 (Fig. 2.4a) and $CO:N_2$=1:6 (Fig. 2.4b) at a gas density 0.12 Amagat. Output coupling of the diffraction grating G3 is presented in Fig. 2.4c. When using the $CO:N_2$ gas mixture, laser efficiency came up to ~ 0.6% (Fig. 2.4b) at 3.8 μm. For the CO:He mixture, laser

efficiency was ~ 0.1%. However, the helium free laser mixture was not good for lasing on higher vibrational bands.

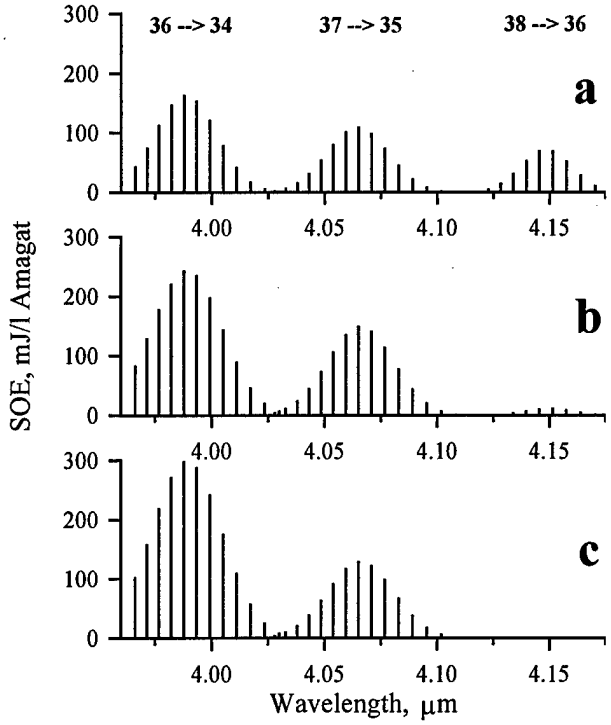

Fig. 2.5. Specific output energy (SOE) vs. wavelength for different content of N_2 in laser mixture: **a** - 0%; **b** - 3.3%; **c** - 10%; SIE=300 J/l Amagat.

To study the influence of the nitrogen admixture on the CO:He laser mixture, measurements of SOE on the high vibrational bands of the FO CO laser spectrum were carried out. Fig. 2.5 demonstrates the ro-vibrational structure of FO CO laser spectrum corresponding to the three vibrational bands 38→36, 37→35, and 36→34 for different content of N_2 in the laser mixture. The initial laser mixture of CO:He = 1:4 with gas density 0.12 Amagat was used (Fig. 2.5a). When nitrogen content increased, the SOE of the 36→34 vibrational transition increased and that of the 38 →36 vibrational transition decreased. When nitrogen content in the gas mixture reached more than 10%, lasing on the 38→36 vibrational transition was not observed at all (Fig. 2.5c). This phenomenon could be explained by quasi-resonant collisional interaction between the 38→36 vibrational transition of CO and the 0→1 vibrational transition of N_2 (40→38 CO and 0→1 N_2 are exactly resonant). As a result, with grating G3 the longest wavelength obtained for the CO:He=1:4 gas mixture was 4.16 μm (Fig. 2.4a, 38→36 transition) and 4.03 μm (Fig. 2.4b, 37→35 transition) for the CO:N_2=1:6 gas mixture.

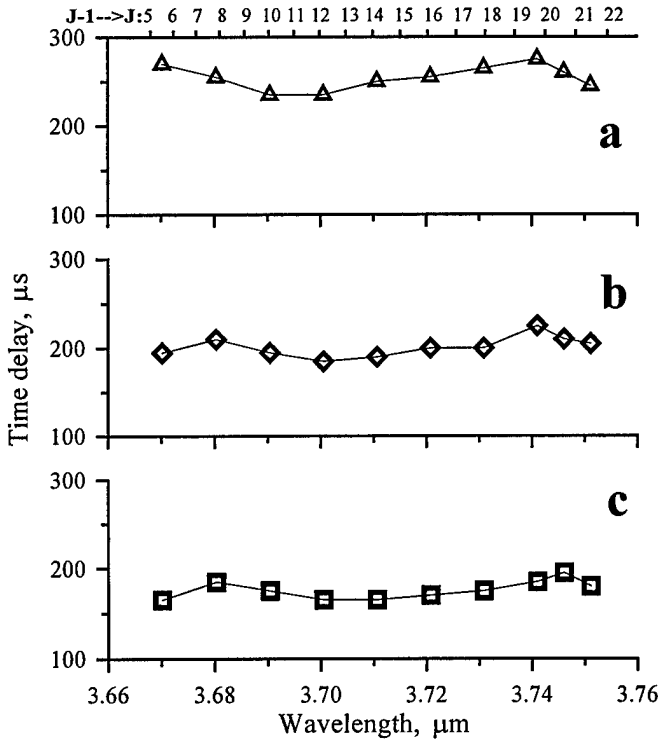

Fig. 2.6. Time delay vs. wavelength and rotational quantum number J for various SIE: 300 (a), 400 (b) and 540 (c) J/l Amagat. Gas mixture CO:N_2=1:9, N=0.12 Amagat. Grating G1. Vibrational band 32→30.

By using the three gratings G1-G3, frequency tunable single-line FO CO lasing was observed within the spectral region 2.71-4.17 μm on 413 ro-vibrational lines (**Table** 2.1). It should be noted that lack of lasing at wavelengths shorter than ~2.7 μm can be explained by absorption of laser radiation by atmospheric water vapor in the resonator in the 0.4 m spacing between the Brewster window and the grating.

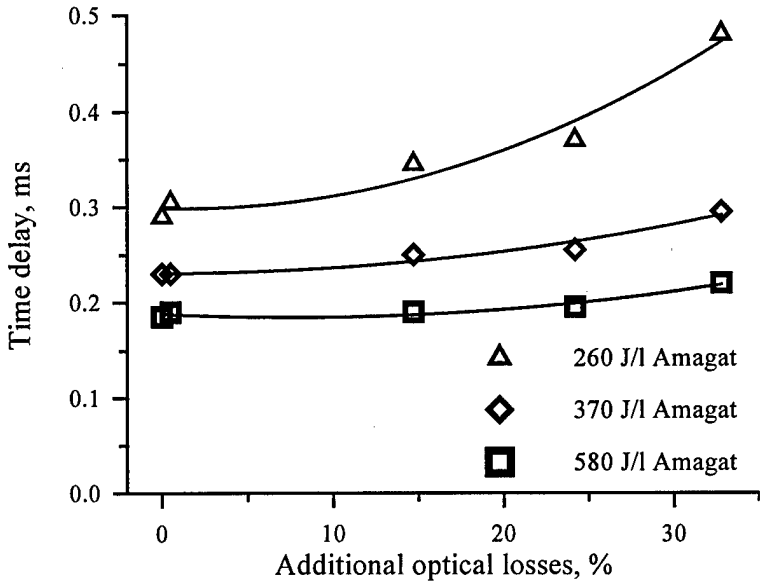

Fig.2.7. Time delay vs. additional optical losses for different SIE (260, 370 and 580 J/l Amagat). Laser wavelength was 3.84 μm. Experimental conditions correspond to Fig.2.2.

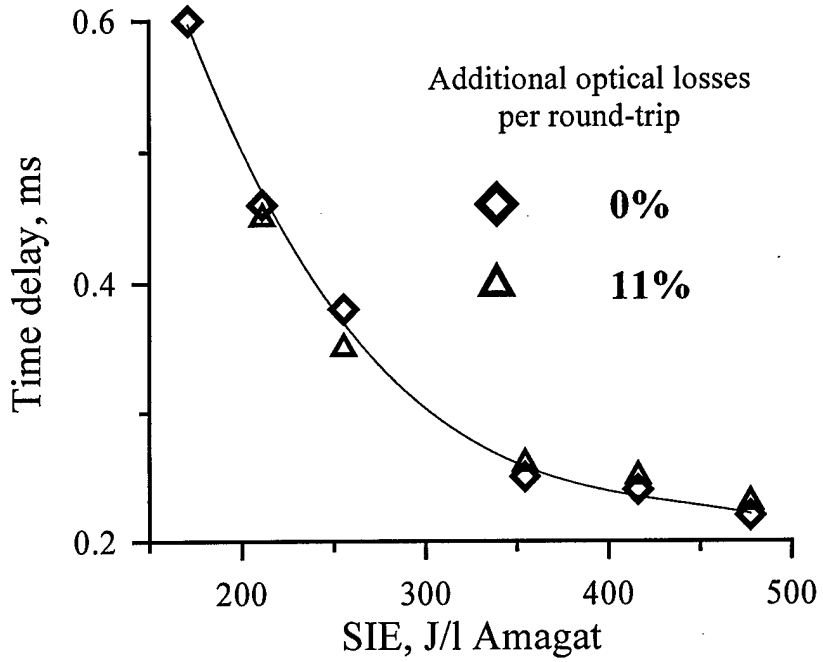

Fig.2.8. Time delay vs. specific input energy (SIE) for different magnitudes of additional optical losses. Wavelength 3.84 μm. Experimental conditions correspond to Fig.2.2.

Fig. 2.1b demonstrates time delay τ_d between the beginning of the pump and radiation pulses versus laser wavelength for the experimental conditions corresponding to Fig. 2.1a. When wavelength increased from 2.9 up to 4.1 μm, time delay increased monotonously from ~60 up to ~350 μs, in contrast with the output coupling curve (Fig. 2.1c). The time delay was approximately the same for lasing on different rotational transitions within each vibrational band at fixed SIE (Fig. 2.6a-c). With varying additional optical losses introduced by intracavity CaF_2 flat plate from 0% up to 33% (laser wavelength 3.84 μm, experimental conditions correspond to Fig.2.2), the time delay was not considerably changed for high SIE (370 and 580 J/l Amagat) much higher than threshold SIE (Fig.2.7). For relatively low additional optical losses (~11%), the time delay did not change at all even at low SIE (~200 J/l Amagat) (Fig.2.8). These facts indicate that time delay is dominated by transient kinetic processes and, to a lesser degree, by lasing build-up time. Single-line FO CO laser pulse length τ and time delay for a select line strongly depended on gas density in the active medium and SIE. Figs. 2.9a, b demonstrate a dependence τ and reverse time delay ($1/\tau_d$) on gas density for selected ro-vibrational transition 36→34 P(13) at two different values of SIE. Reverse delay time was practically linear with gas density rise. Single-line pulse length decreased from ~ 2 ms for a gas density 0.05 Amagat down to ~ 0.5 ms for N = 0.3 Amagat. The dependence of τ_d on SIE for selected ro-vibrational line 32→30 P(10) is presented in Fig. 2.10. It is ~ 1 ms for SIE close to threshold (~100 J/l Amagat) and ~ 0.2 ms for a SIE of 600 J/l Amagat.

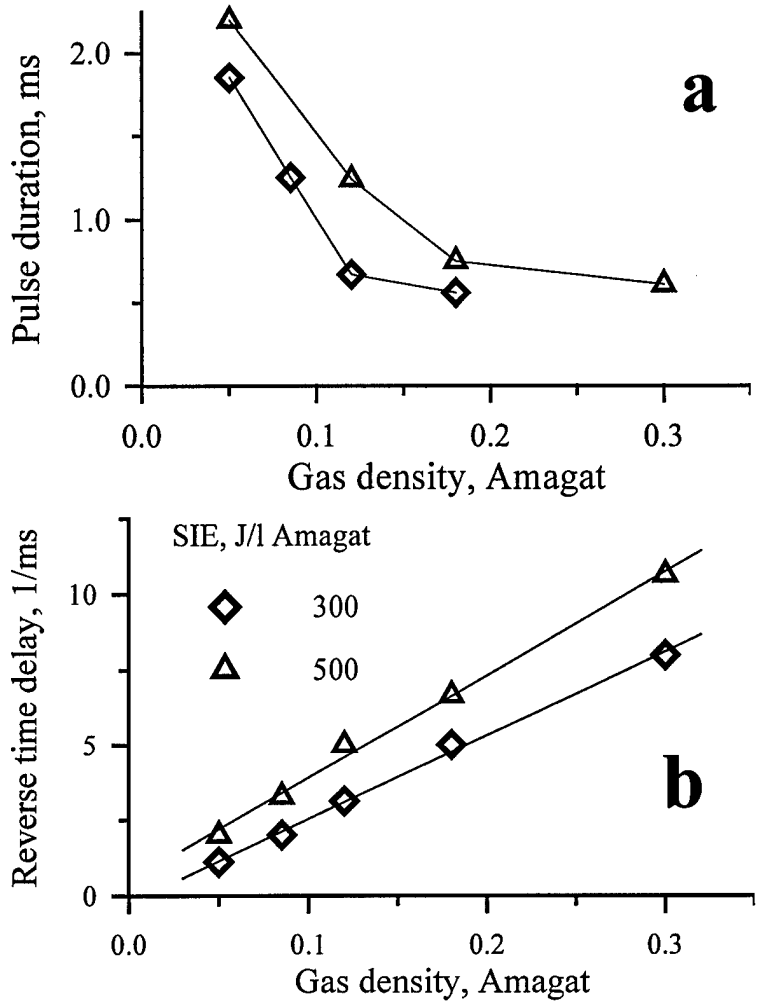

Fig. 2.9. Pulse duration (a) and reverse time delay (b) vs. gas density for two SIE (300 and 500 J/l Amagat). Gas mixture $CO:N_2$=1:9. Grating G1. Ro-vibrational transition 36→34 P(13).

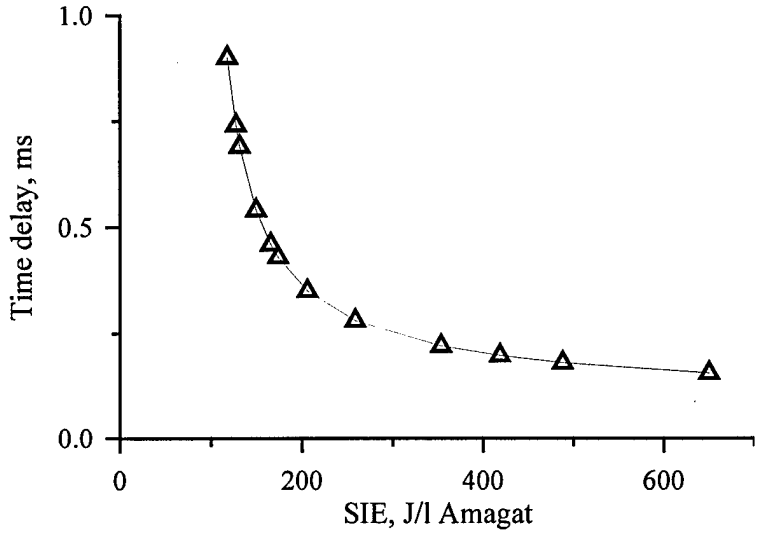

Fig. 2.10. Time delay vs. specific input energy (SIE). Gas mixture $CO:N_2$=1:9. Grating G1. Ro-vibrational transition 32→ 30 P(10)

Dependencies of SOE on SIE for FO CO lasing on selected ro-vibrational transition 35→33 P(12) for five different gas mixtures are presented in Fig. 2.11. The lowest SOE was obtained for the CO:He mixture. An increased SOE was obtained for the $CO:N_2$:He mixture. The highest SOE was obtained for the $CO:N_2$ mixtures. It should be noted that threshold SIE increased as the content of CO in the $CO:N_2$ mixture increased. The dependence of SOE on SIE reached a maximum for the $CO:N_2$=1:9 laser mixture, which can be explained by overheating of laser mixture. The position of

the maximum depended on the gas density for each ro-vibrational line. Fig. 2.12 demonstrates SOE versus SIE for three ro-vibrational lines of vibrational transition 36→34 (laser mixture $CO:N_2$=1:9). The lower the gas density and the higher the rotational transition involved, the higher the SIE that was needed to reach the maximum.

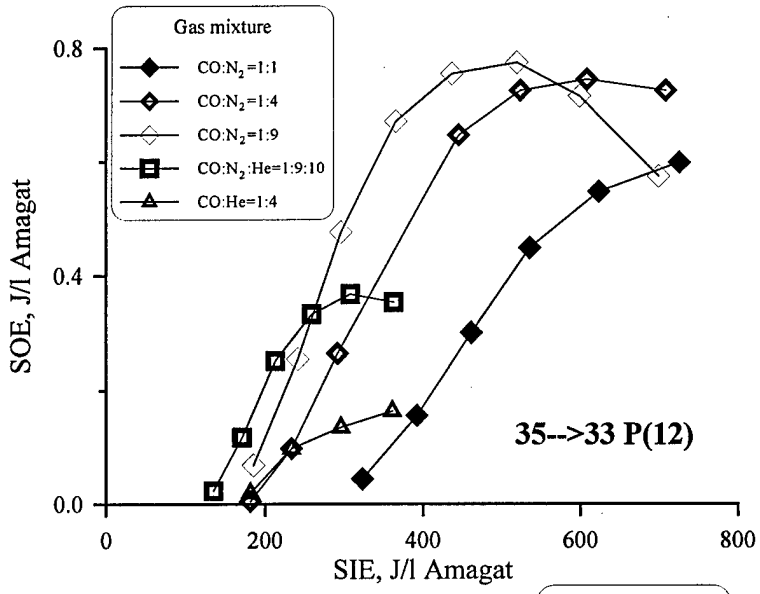

Fig. 2.11. Specific output energy (SOE) vs. specific input energy (SIE) for different gas mixtures. Ro-vibrational transition 35→33 P(12). Grating G1. N=0.12 Amagat.

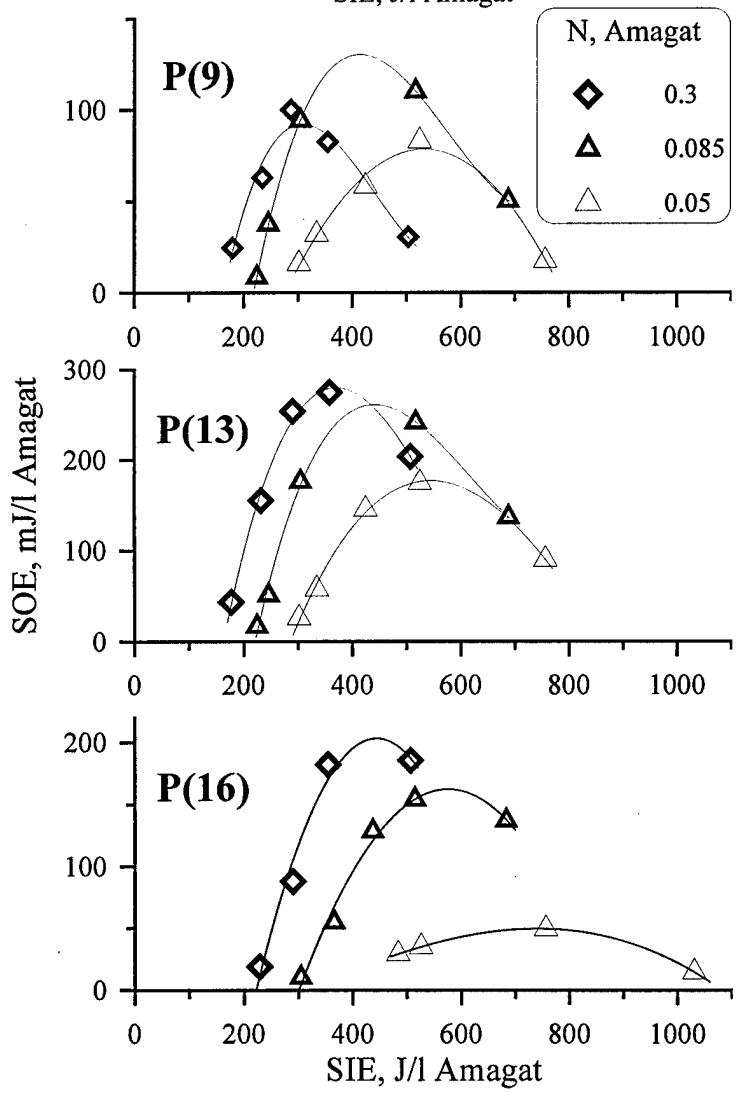

Fig. 2.12. Specific output energy (SOE) vs. specific input energy (SIE) for different gas density. $CO:N_2$=1:9. Ro-vibrational transition 36→34 P(9), P(13), and P(16).

The dependencies of SOE at SIE=230 J/l Amagat and threshold SIE on rotational quantum number J within the 35→33 vibrational band are presented in Figs. 2.13a, b. A laser mixture $CO:N_2:He=1:9:10$ at a gas density 0.12 Amagat was used. The SOE for the center of the band (ro-vibrational line P(11)) is higher than 0.3 J/l Amagat. Output efficiency reached 0.14% for the 35 →33 P(11) and P(12) lines. Fig. 2.13a demonstrates the experimentally measured SOE (bars) and experimental data approximated by a Gaussian curve (solid line). One can see the Gaussian approximation correlates well with the experimental data. The dependence of threshold SIE on rotational quantum number was asymmetric with respect to the central line. As the rotational quantum number of the laser transition increased, i. e., from P(14) up to P(19), the threshold SIE increased two fold. However, as P(J) changed from P(14) down to P(5), quite different situation was observed: threshold SIE was unchanged, remaining 100-120 J/l Amagat. This same behavior was also observed for other vibrational bands.

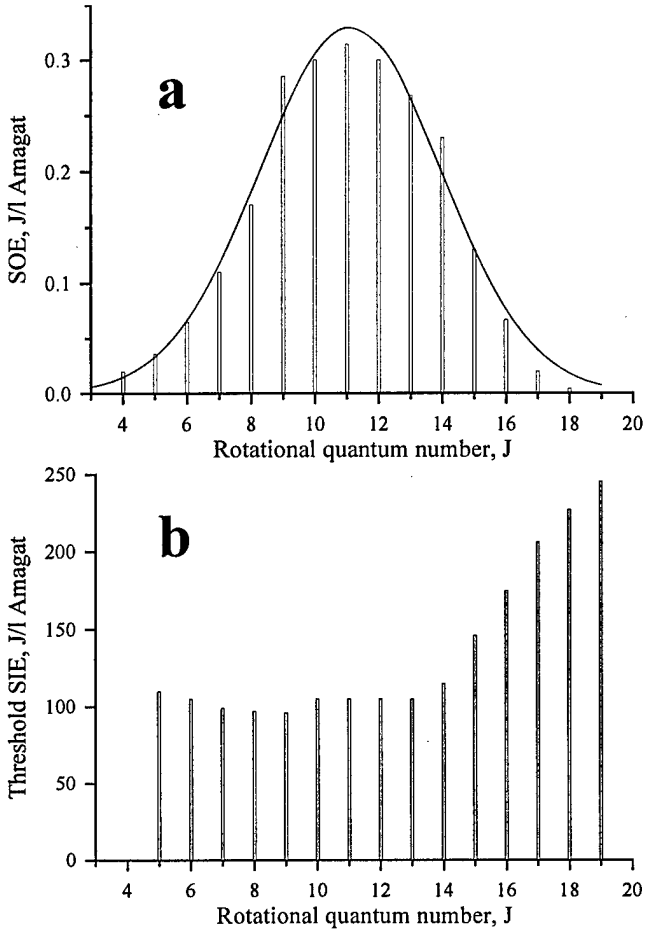

Fig. 2.13. Specific output energy (SOE) at SIE=230 J/l Amagat (a) and threshold SIE (b) vs. rotational quantum number J. Vibrational band 35→33; $CO:N_2:He=1:9:10$; 0.12 Amagat.

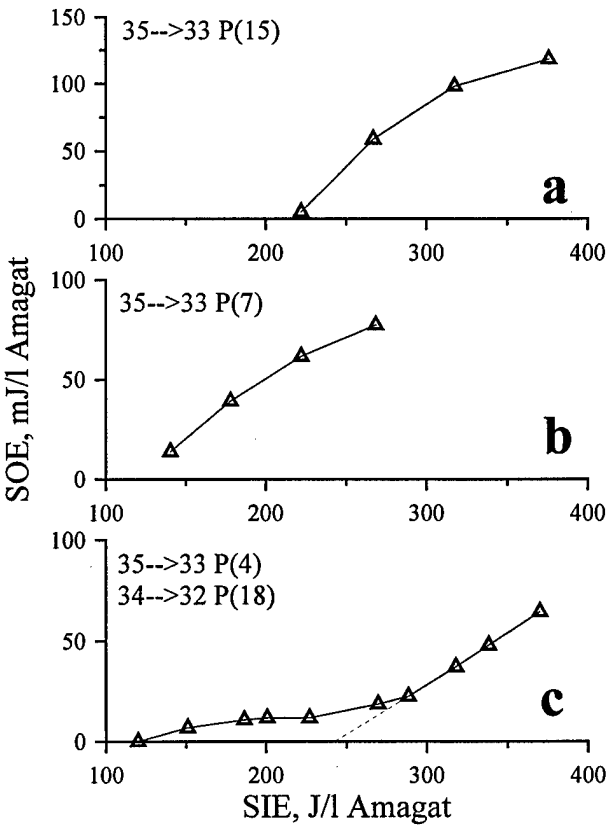

Fig. 2.14. Specific output energy (SOE) vs. specific input energy (SIE) for different ro-vibrational transitions. $CO:N_2:He=1:9:10$; N=0.12 Amagat; T=100 K (Ionin et al., 1999a)

Simultaneous lasing on adjacent vibrational transitions and on different rotational lines with a wavelength difference that was beyond the spectral resolution of the laser optical scheme was also

experimentally observed. For example, the 31→29 P(20) and 32→30 P(7) transitions with theoretically calculated wavelengths of 3.6768 and 3.6766, respectively. Lasing on the two ro-vibrational transitions was detected by the threshold SIE difference. Figs. 2.14a, b (Ionin et al., 1999a) demonstrates SOE versus SIE for different P(J) (J=15 and 7) in the 35→33 vibrational band. For 33 P(15), threshold lasing took place at SIE 220 J/l Amagat, whereas for the 33 P(7) line, threshold was at 130 J/l Amagat. The dependencies in Figs. 2.14a, b are monotonous. Fig. 2.14c demonstrates the dependence of SOE at a wavelength where two FO CO laser rotational lines occur, although they correspond to two different adjacent vibrational bands within the spectral resolution of the laser optical scheme: namely 33 P(4) and 32 P(18). As SIE increases, 33 P(4) FO CO lasing starts at a low SIE of ~120J/l Amagat, which is typical for laser transitions with lower J. Typical monotonous dependence of SOE on SIE (compare Figs. 2.14b and c) is observed up to a SIE of 250 J/l Amagat. At this point, abrupt growth is observed. This phenomenon is considered to be the appearance of lasing on the 34→32 P(18) line, which has a threshold SIE of ~250 J/l Amagat. This same analysis of SOE dependence upon SIE was also used for estimation of threshold SOE at other wavelengths where simultaneous lasing occurred on different rotational lines that belonged to adjacent vibrational bands. It should be noted that the above effect was not observed for adjacent 35 →33 and 36→34 vibrational bands, as lasing on the 36→34 band took place with lower SIE and within a more narrow interval of rotational lines J as compared to the 35→33 band. Dependence of SOE on wavelength, with SIE being 540 J/l Amagat, within the spectral interval corresponding to three vibrational bands (32→30, 31→29 and 30→28) is presented in Fig. 2.15. The solid line in the figure is the sum of three Gaussians corresponding to the three vibrational bands. This curve is in good agreement with the experimental data.

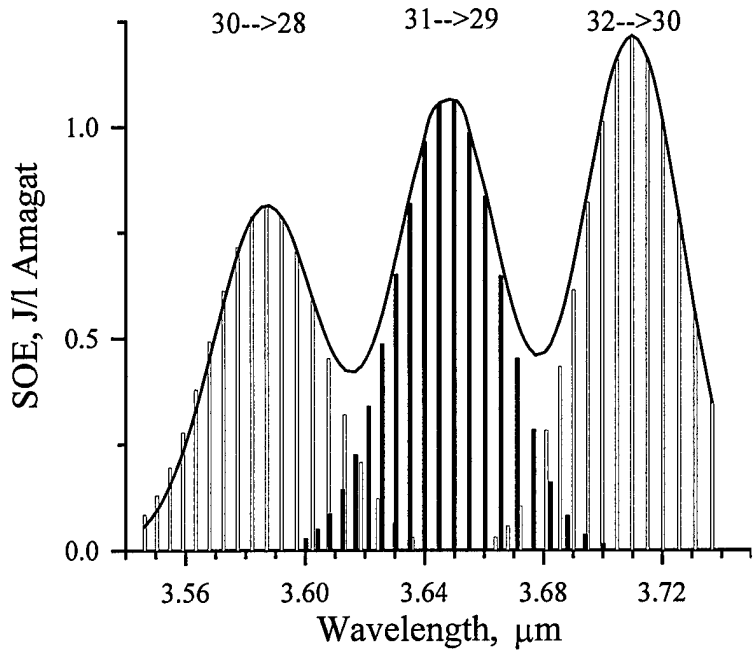

Fig. 2.15. Specific output energy (SOE) vs. wavelength within spectral interval corresponding to three vibrational transitions. Solid line is a sum of three Gaussians. CO:N_2=1:9; 0.12 Amagat; SIE=540 J/l Amagat.

Fig. 2.16(a-c) demonstrates SOE versus rotational quantum number J within the 32→30 vibrational band for increasing SIE (solid lines are the Gaussians). The J value at which maximum SOE occurred increased with increasing SIE. When the SIE was 200 J/l Amagat (Fig. 2.16a), maximum SOE was observed at J=11, and when the SIE was raised to 670 J/l Amagat, maximum SOE was at J=15 (Fig. 2.16c). This can be explained by an increased threshold SIE for higher J and a rise in gas temperature (which provides a more favorable condition for lasing on higher J) with increasing SIE.

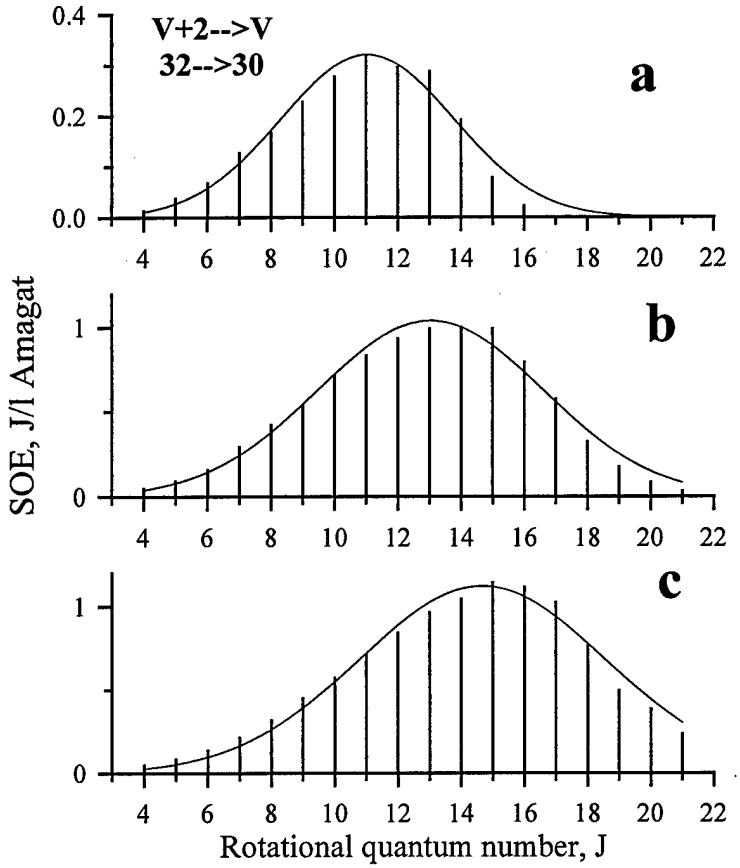

Fig. 2.16. Specific output energy (SOE) vs. rotational quantum number J for increasing specific input energy (SIE): 200 (a), 400 (b), 670 (c) J/l Amagat. Vibrational band 32→30; CO:N_2 =1:9; 0.12 Amagat.

2.4. Kinetic model

2.4.1. General description of the kinetic model

A multi-quantum kinetic model, which is very important in describing a FO CO laser operating on highly excited vibrational levels [Ionin et al., 1996b, 1998e, 1999c,d], was used for modeling the single-line FO CO laser and the results were compared to those obtained by using a single quantum exchange model. Except for multi-quantum VV exchange processes in CO gas, the kinetic model is described in [Ionin et al., 1997a, 1998b]. Thus, only the part of the kinetic model that represents VV exchange is described below. Schematically, the system of kinetic equations describing the time evolution of vibrational level **v** of CO molecule populations has the form:

$$\frac{dn_v}{dt} = R^v_{e-V} + R^v_{VV} + R^v_{VV'} + R^v_{VT} + R^v_{SP} + R^v_{IND}. \qquad (1)$$

Here, R^v_{e-V}, $R^v_{VV'}$, R^v_{VT}, R^v_{SP}, R^v_{IND} are the rates of electron-molecule excitation, inter-molecular vibration-vibration exchange, vibration relaxation, and spontaneous and induced radiative transitions. Their detailed expressions can be found in [Belykh et al., 1995] and are not reproduced here. The components of the kinetic equation corresponding to multi-quantum VV exchange are:

$$R^v_{VV} = \sum_{m\geq 1}(W_{v+m,v}n_{v+m} + W_{v-m,v}n_{v-m} - (W_{v,v+m} + W_{v,v-m})n_v, \qquad (2)$$

where $W_{v+m,v}$ is the frequency of transitions from the level **v+m** to the level **v** in processes of type (1). It is expressed as follows:

$$W_{v+m,v} = \sum_{i \geq m} Q_{i-m,i}^{v+m,v} n_i , \qquad (3)$$

where $Q_{i-m,i}^{v+m,v}$ are the rate constants of **m**-quantum exchange. As concluded from [Ionin et al., 1996b, 1998e, 1999c,d] and [Billing, 1986], processes with **m**>4 are unimportant for **v**< 30-35 and were not considered.

2.4.2. First-overtone CO laser characteristics

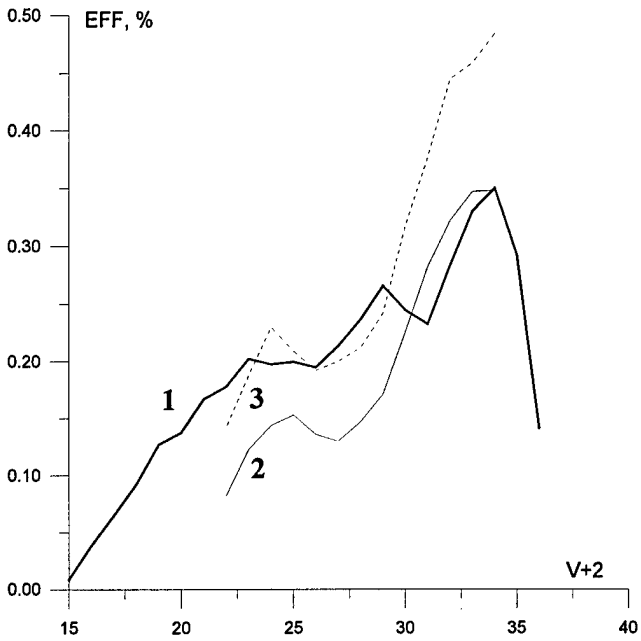

Fig. 2.17. Output laser efficiency for the FO CO laser with diffraction grating G2 vs. vibrational transition V+2→V.
1 - experiment, 2, 3 - results of simulation by MQE model. (2 - additional losses 7.5%, 3 - additional losses 5.5%)

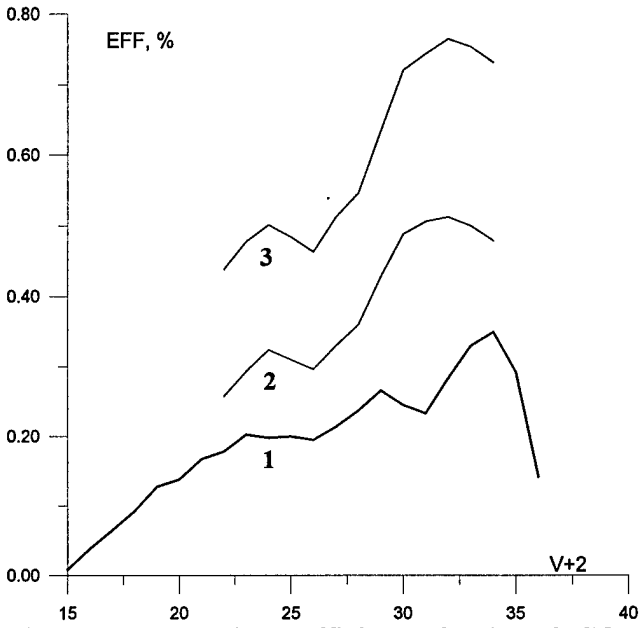

Fig. 2.18. Output laser efficiency for the FO CO laser with diffraction grating G2 vs. vibrational transition V+2→V.
1 - experiment, 2, 3 - results of simulation by SQE model. (2 - additional losses 7.5%, 3 - additional losses 5.5%)

Theoretical simulations were performed for the same experimental conditions using two versions of the model for V-V exchange: multi-quantum exchange (MQE) and single-quantum exchange (SQE) models. The first one is more preferable following basic physical assumptions [Ionin et al., 1996b, 1998e, 1999c,d] and [Billing, 1986], since the selective FO CO laser operates on very high vibrational transitions (up to V+2→V=38→36). The SQE model [Ionin et al., 1997a, 1998b] normally used for modeling the CO laser was applied to clarify its applicability via comparison with the results obtained from the MQE model and the experiment. The modeling was done for two gas mixtures ($CO:N_2$=1:9 and $CO:N_2$=1:6) from which the best energy characteristics were obtained with gratings G2 and G3 (see Figs.2.4a, 2.5b). For the model, laser mixture, pump,

and resonator parameters were set to those used in the experimental measurements: SIE=360 J/l Amagat, T=100 K, N=0.12 Amagat for CO:N_2=1:9, and SIE=500 J/l Amagat, T=100 K, N=0.12 Amagat for CO:N_2=1:6. The output coupling values used corresponded to the results in Figs. 2.4b, 2.5c. Unfortunately, there was no exact data on cavity optical losses associated with scattering and absorption introduced by the grating. Therefore, these useless cavity losses were taken as a fixed parameter, assuming it to be independent of the wavelength.

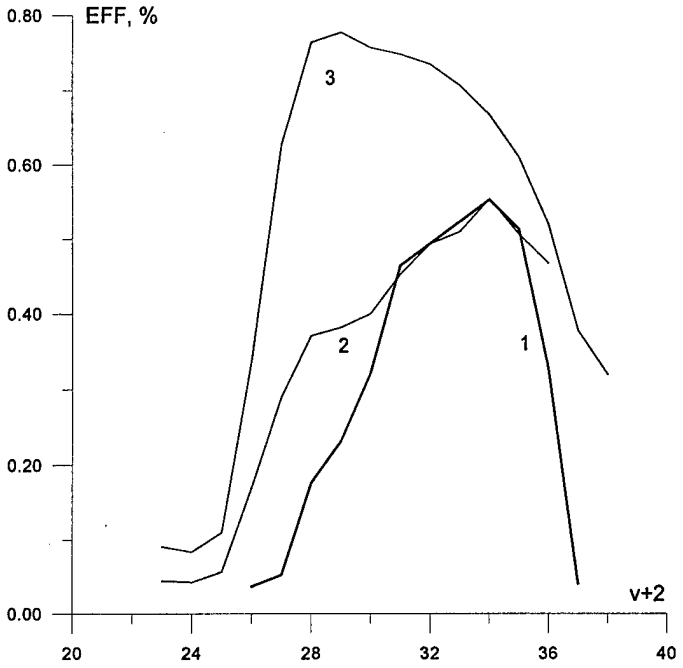

Fig. 2.19. Output laser efficiency for the FO CO laser with diffraction grating G3 vs. vibrational transition V+2→V. 1 - experiment, 2, 3 - results of simulation by MQE and SQE models. (2 - MQE, 3 - SQE)

For round-trip additional losses of 7.5% and 5.5% the tuning curves (i.e., the dependency of output efficiency on vibrational number V+2 for the transition V+2→V) calculated by the MQE model for the CO:N_2=1:9 mixture are compared with experimental results in Fig. 2.17. One can see that agreement with the experiment improves if it is assumed that the additional losses rise with the vibrational quantum number of the selected transition. The results obtained from the SQE model for the same conditions (see Fig. 2.18) are characterized by similar curve shapes, but give much higher output efficiency. The results of calculations for CO:N_2=1:6 are more sensitive to the choice of kinetic model. For round-trip additional losses of 6.8% the tuning curves calculated by the MQE and SQE models are compared with the experimental curve in Fig. 2.19.

It can be clearly seen that the MQE model produces much better agreement with the experimental data than the SQE model based on the shape and amplitude of the tuning curves. Bearing in mind uncertainties associated with a lack of knowledge concerning optical losses (introduced by the grating due to its absorption and scattering) as a function of wavelength, the agreement between predictions and measurements is rather good. Note that there is a higher predicted efficiency for the highest laser transitions. This may be explained by the fact that we did

not take into consideration an influence of the V-V exchange process in which two vibrational quanta in highly excited CO molecule convert into one vibrational quantum in the first excited state of CO or N_2.

2.5. Conclusions

Experiments with a pulsed FO CO laser using a diffraction grating as a frequency selective intracavity optical element demonstrated the feasibility of developing a frequency tunable single-line pulsed FO CO laser. Tunable FO CO lasing on wavelengths from 2.7 up to 4.2 μm corresponding to overtone vibrational transitions from 13→11 up to 38→36 on 413 ro-vibrational lines was experimentally obtained. A parametric study of energetic and spectral characteristics of the single-line FO CO laser was carried out. Energy distribution over ro-vibrational lines was measured. The maximum SOE came up to 2.8 J/l Amagat, with single-line output efficiency being up to 0.6%. For the first time, a multi-quantum theoretical model was used to describe the tunable single-line FO CO laser. This multi-quantum approach demonstrated better agreement between theoretical calculations and observed experimental data for laser output as a function of vibrational quantum numbers.

Table 2.1. Single-line FO CO laser wavelengths theoretically calculated in accordance with [Guelachvili et al., 1983] that correspond to experimentally observed ro-vibrational lines.

J	λ, μm
12→10	
11	2.7054
12	2.7085
13	2.7117
14	2.7149
15	2.7182
13→11	
10	2.7401
11	2.7433
12	2.7464
13	2.7497
14	2.7530
15	2.7563
16	2.7598
14→12	
7	2.7697
8	2.7727
9	2.7758
10	2.7789
11	2.7821
12	2.7853
13	2.7886
14	2.7920
15	2.7954
16	2.7989
17	2.8025
18	2.8061
19	2.8098
15→13	
7	2.8093
8	2.8123
9	2.8155
10	2.8187
11	2.8219
12	2.8252
13	2.8286
14	2.8320
15	2.8355
16	2.8391
17	2.8427
18	2.8464
19	2.8501
16→14	
9	2.8562
10	2.8594
11	2.8627
12	2.8661

J	λ, μm
13	2.8696
14	2.8731
15	2.8766
16	2.8803
17	2.8840
18	2.8877
19	2.8916
17→15	
8	2.8947
9	2.8979
10	2.9012
11	2.9046
12	2.9081
13	2.9116
14	2.9152
15	2.9188
16	2.9225
17	2.9263
18	2.9301
19	2.9341
20	2.9380
18→16	
7	2.9342
8	2.9375
9	2.9408
10	2.9442
11	2.9476
12	2.9511
13	2.9547
14	2.9584
15	2.9621
16	2.9659
17	2.9697
18	2.9737
19→17	
6	2.9748
7	2.9780
8	2.9814
9	2.9848
10	2.9882
11	2.9917
12	2.9953
13	2.9990
14	3.0027
15	3.0065
16	3.0104
17	3.0143

J	λ, μm
20→18	
6	3.0198
7	3.0231
8	3.0265
9	3.0299
10	3.0334
11	3.0370
12	3.0407
13	3.0445
14	3.0483
15	3.0522
16	3.0561
17	3.0602
18	3.0643
21→19	
6	3.0659
7	3.0693
8	3.0728
9	3.0763
10	3.0799
11	3.0836
12	3.0873
13	3.0912
14	3.0951
15	3.0990
16	3.1031
17	3.1072
18	3.1114
22→20	
5	3.1100
6	3.1134
7	3.1168
8	3.1204
9	3.1240
10	3.1277
11	3.1314
12	3.1352
13	3.1392
14	3.1431
15	3.1472
16	3.1513
23→21	
4	3.1553
5	3.1587
6	3.1621
7	3.1657
8	3.1693

J	λ, μm
9	3.1730
10	3.1767
11	3.1806
12	3.1845
13	3.1885
14	3.1926
15	3.1967
16	3.2010
17	3.2053
18	3.2097
24→22	
4	3.2053
5	3.2088
6	3.2123
7	3.2159
8	3.2196
9	3.2234
10	3.2272
11	3.2311
12	3.2352
13	3.2392
14	3.2434
15	3.2477
16	3.2520
17	3.2564
25→23	
4	3.2568
5	3.2603
6	3.2639
7	3.2676
8	3.2714
9	3.2752
10	3.2792
11	3.2832
12	3.2873
13	3.2915
14	3.2957
15	3.3001
16	3.3045
17	3.3091
18	3.3137
19	3.3184
20	3.3231
21	3.3280
26→24	
4	3.3098
5	3.3134

J	λ, μm
6	3.3170
7	3.3208
8	3.3247
9	3.3286
10	3.3326
11	3.3367
12	3.3409
13	3.3452
14	3.3496
15	3.3541
16	3.3586
17	3.3632
18	3.3680
19	3.3728
20	3.3777
21	3.3827
27→25	
4	3.3643
5	3.3680
6	3.3718
7	3.3756
8	3.3796
9	3.3836
10	3.3877
11	3.3919
12	3.3962
13	3.4006
14	3.4051
15	3.4096
16	3.4143
17	3.4190
18	3.4239
19	3.4288
20	3.4338
21	3.4390
22	3.4442
28→26	
4	3.4205
5	3.4243
6	3.4282
7	3.4321
8	3.4361
9	3.4403
10	3.4445
11	3.4488
12	3.4532
13	3.4577

J	λ, μm
14	3.4623
15	3.4669
16	3.4717
17	3.4766
18	3.4815
19	3.4866
20	3.4918
21	3.4970
22	3.5024
23	3.5078
29→27	
4	3.4785
5	3.4824
6	3.4863
7	3.4903
8	3.4945
9	3.4987
10	3.5030
11	3.5074
12	3.5119
13	3.5165
14	3.5212
15	3.5260
16	3.5309
17	3.5359
18	3.5410
19	3.5462
20	3.5515
21	3.5569
22	3.5624
23	3.5679
24	3.5736
30→28	
4	3.5383
5	3.5423
6	3.5463
7	3.5504
8	3.5547
9	3.5590
10	3.5634
11	3.5679
12	3.5726
13	3.5773
14	3.5821
15	3.5870
16	3.5920
17	3.5971

J	λ, μm
18	3.6024
19	3.6077
20	3.6131
21	3.6186
22	3.6243
23	3.6300
24	3.6359
31→29	
4	3.6001
5	3.6041
6	3.6082
7	3.6125
8	3.6168
9	3.6212
10	3.6258
11	3.6304
12	3.6351
13	3.6400
14	3.6449
15	3.6500
16	3.6551
17	3.6604
18	3.6657
19	3.6712
20	3.6768
21	3.6825
22	3.6882

J	λ, μm
23	3.6941
24	3.7001
32→30	
4	3.6639
5	3.6680
6	3.6723
7	3.6766
8	3.6810
9	3.6856
10	3.6902
11	3.6950
12	3.6998
13	3.7048
14	3.7099
15	3.7151
16	3.7203
17	3.7257
18	3.7312
19	3.7368
20	3.7426
21	3.7484
22	3.7544
23	3.7604
24	3.7666
33→31	
4	3.7299
5	3.7341

J	λ, μm
6	3.7385
7	3.7429
8	3.7474
9	3.7521
10	3.7569
11	3.7618
12	3.7667
13	3.7718
14	3.7770
15	3.7824
16	3.7878
17	3.7933
18	3.7990
19	3.8048
20	3.8106
21	3.8166
22	3.8227
23	3.8290
34→32	
4	3.7982
5	3.8025
6	3.8070
7	3.8115
8	3.8162
9	3.8210
10	3.8259
11	3.8309

J	λ, μm
12	3.8360
13	3.8412
14	3.8466
15	3.8520
16	3.8576
17	3.8633
18	3.8691
19	3.8751
20	3.8811
21	3.8873
22	3.8936
23	3.9000
35→33	
4	3.8689
5	3.8734
6	3.8779
7	3.8826
8	3.8874
9	3.8923
10	3.8973
11	3.9025
12	3.9077
13	3.9131
14	3.9186
15	3.9242
16	3.9300
17	3.9358

J	λ, μm
18	3.9418
19	3.9479
20	3.9541
21	3.9605
22	3.9669
23	3.9735
24	3.9803
36→34	
4	3.9423
5	3.9468
6	3.9515
7	3.9563
8	3.9612
9	3.9663
10	3.9715
11	3.9767
12	3.9821
13	3.9877
14	3.9933
15	3.9991
16	4.0050
17	4.0110
18	4.0172
19	4.0235
20	4.0299
21	4.0364
37→35	

J	λ, μm
6	4.0279
7	4.0328
8	4.0379
9	4.0431
10	4.0484
11	4.0538
12	4.0594
13	4.0651
14	4.0709
15	4.0768
16	4.0829
17	4.0891
18	4.0954
19	4.1019
38→36	
10	4.1283
11	4.1339
12	4.1396
13	4.1455
14	4.1515
15	4.1576
16	4.1639
17	4.1703

3. Gain characteristics of FO CO laser

3.1. Introduction

Generally, small signal gain (SSG) for ro-vibrational-transitions in P-branch can be calculated from the well-known formulae

$$g_{V,j}=\sigma_{v,j}(N_{V+2}-\delta_{V,J}N_V),$$

$$\sigma_{v,j} = (\lambda^2/8\pi)\, A_{V+2,\,v}\, J\, \frac{B_{v+2}}{kT} \exp(-\frac{B_{v+2}F(J-1)}{kT})\; G(\lambda),$$

$$\delta_{V,J} = (B_V/\, B_{V+2})\exp([-B_V F(J) + B_{V+2}F(J\text{-}1)]/kT).$$

Here $\sigma_{V,J}$ is the effective stimulated emission cross section (SECS) for the transition $V+2 \rightarrow V$, $J-1 \rightarrow J$ and is related to the population N_{V+2} on the vibrational level $V+2$. Other quantities are defined in [Ionin et al., 1997a].

Quite valuable information can be obtained from data on SSG, especially from its time characteristics, namely data on inversion population, which can give information concerning CO laser kinetics.

Data on saturation gain, which can give information on saturation intensity are also very valuable, because information about relaxation time, determined by V-V exchange in case of CO laser, can be extracted, in principle. Because, CO laser is not a simple two-level system, but complicated multilevel laser system, some analysis and definition of saturated gain characteristics are needed. Results on gain measurements, theoretical analysis of amplification characteristics, and possibilities to employ CO MOPA system for kinetic studies are discussed in this part of the Report.

3.2. Small signal gain measuring through threshold lasing

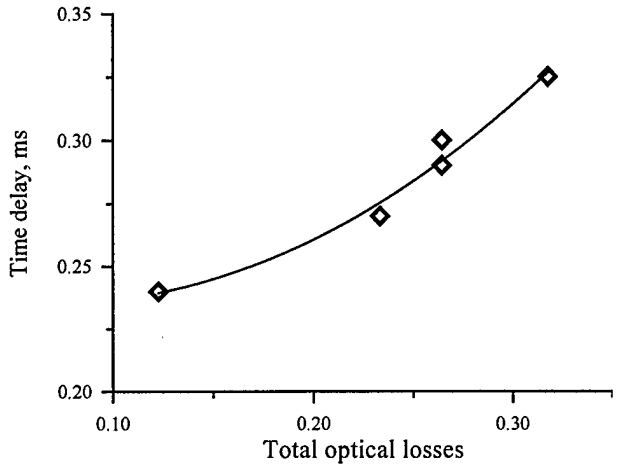

Fig.3.1. Time delay vs. total optical losses.
P(14) 30→28, CO:N_2=1:9, N=0.12 Amagat,
SIE=630 J/l Amagat

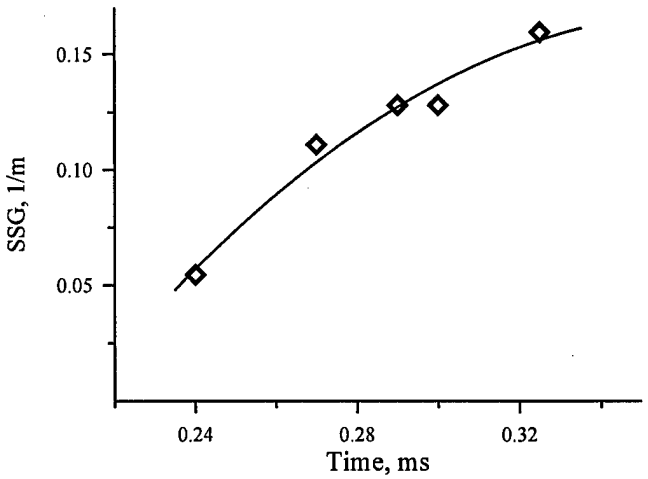

Fig.3.2. Temporal behavior of single-line SSG.Experimental conditions correspond to Fig.3.1

To determine the temporal behavior of single-line SSG a time delay i.e. a time interval needed for SSG to reach its threshold value (and for laser pulse build-up), was measured as a function of the total optical losses (Fig.3.1) at the following experimental conditions: P(14) 30→28, $CO:N_2$=1:9; SIE=630 J/l Amagat; N = 0.12 Amagat. Additional optical losses were introduced by placing a flat plate made of CaF_2 and spectral filter made of thin (~0.5 mm) fused silica into the FO CO laser resonator under changeable angle to the laser optical axis. Fig.3.2 demonstrates the dependence of single-line SSG on time, that was obtained by using data of Fig.3.1 neglecting time of laser pulse build-up. SSG for the high transition 30→28 exceeded 1.5 10^{-3} cm^{-1}, which was achieved 300 μs later than pump pulse started.

3.3. Master-oscillator-power amplifier FO and FB CO laser system

3.3.1. Amplification of multiline signal

Preliminary experimental research of small signal gain (SSG) on FO transitions (V+2→V) with multiline input spectrum was carried out by using MOPA system. Another cryogenically cooled pulsed laser installation with active medium length of 1.5 m was used as master oscillator. Optical resonator consisted of two dielectric mirrors (M92 and M99). Optical volume was about 1.0 *l*. Specific input energy was 250 J/l Amagat. Laser mixture $CO:N_2$=1:9 at gas density of 0.14 Amagat was used. FO CO laser ran on vibrational transitions from 13→11 up to 17→15 (see Fig.3.3). Output energy was about 100 mJ (~0.7 J/l Amagat) with output pulse duration about 500 μs.

FO CO laser MOPA system was launched for the first time. Gas mixture $CO:N_2$=1:9 with gas density of 0.12 Amagat was used in the power amplifier. The dependence of the laser gain on SIE deposited into the laser amplifier is presented in Fig.3.4. Laser gian achieved 0.12 m^{-1} for SIE 620 J/l Amagat. There is a good agreement between the SSG obtained in the experiment and the value estimated in [Ionin et al., 1997a].

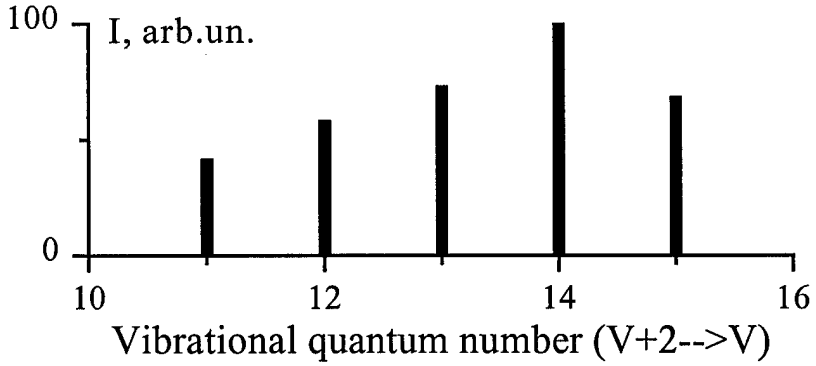

Fig.3.3. Output spectrum of FO CO master oscillator

Fig.3.5 demonstrates the dependence of gain on time delay between the beginnings of pump (electric discharge) pulse of the laser amplifier and the master-oscillator for the same experimental

conditions ($CO:N_2$ = 1:9; gas density ~0.12 Amagat, spectrum of input signal consists of FO CO laser vibrational band V+2→V, where V=11 - 15). One can see that maximum gain up to 0.08 m^{-1} is observed, when MO pulse enters the PA 100-200 μs later than amplifier pump pulse.

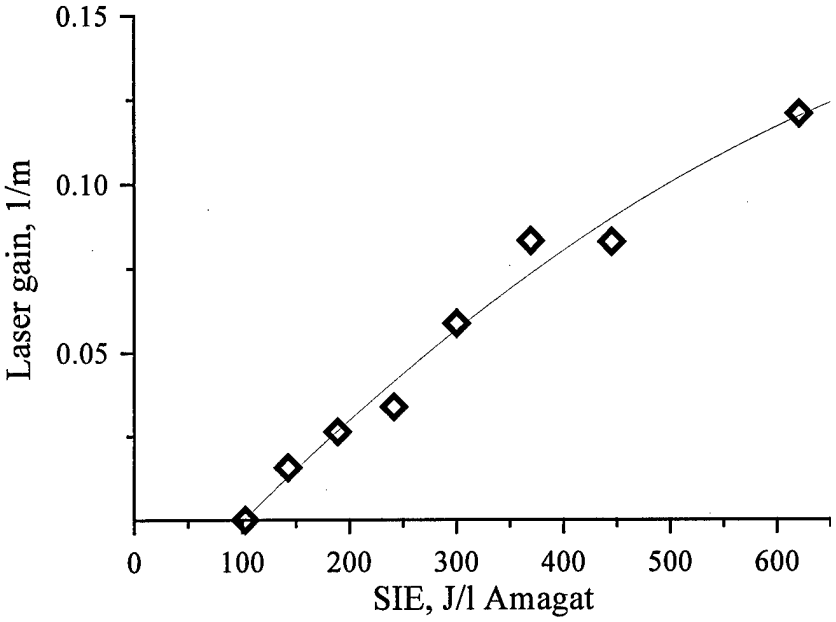

Fig.3.4. Gain vs. specific input energy (SIE) deposited into the laser amplifier
Average input intensity I_{in} = 30 W/cm^2,
input pulse duration τ_{pul} = 500 μs
Amplifier medium:
$CO:N_2$ = 1:9;
N = 0.12 Amagat

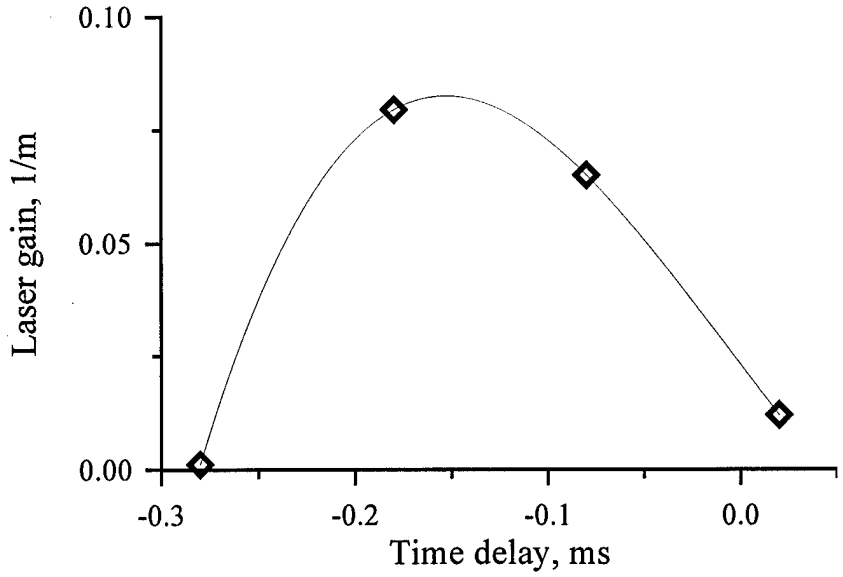

Fig.3.5. Gain vs. time delay between the beginnings of the pump pulse of the laser amplifier and master-oscillator.
Experimental conditions were the same as in Fig.3.4.

3.3.2. Amplification of single-line signal

The gain of the single-line FO CO laser radiation was also measured experimentally. The gas mixture $CO:N_2$ = 1:9 with density 0.16 Amagat was used as the laser medium of the amplifier. The energy of the input signal of the single-line FO CO laser was about 60 mJ. The radiation was directed to the active medium of the laser amplifier by concave mirror. The aperture of the laser beam at the entrance of the laser amplifier was 10 mm in diameter. The dependencies of the gain on specific input energy (SIE) for two rotational-vibrational transitions 26→24 P(14) and 33→31 P(13) (laser wavelengths 3.35 μm and 3.77 μm, correspondingly) are presented in Fig.3.6.

The measurement of the gain was carried out for simultaneous start of electric discharge in the MO and the amplifier. One can see that gain for the two ro-vibrational transitions are not much different. The maximum single-line gain up to 0.08 - 0.09 m^{-1} was observed, when SIE being about 400 J/l Amagat.

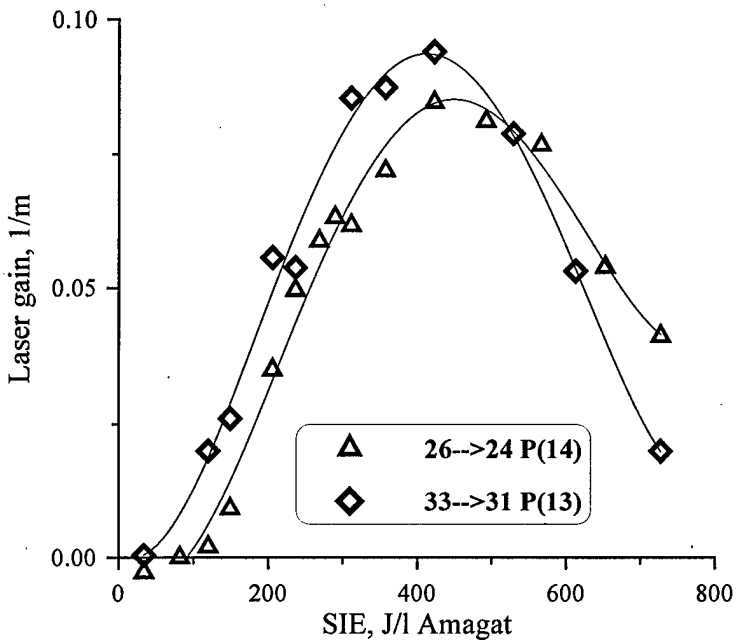

Fig.3.6. Laser gain vs. specific input energy (SIE) for two ro-vibrational transitions 26→24 P(14) and 33→31 P(13) (wavelength 3.35 and 3.77 μm, correspondingly)

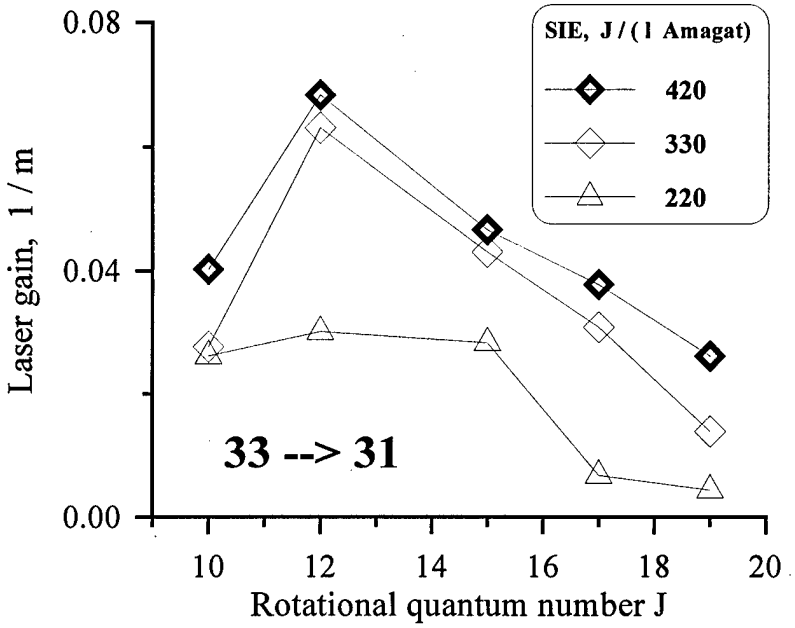

Fig.3.7. Laser gain on 33→31 vibrational transition vs. rotational quantum number for various SIE.

For the FO vibrational transition 33→31 the single-line gain on different rotational lines was measured at three different values of SIE (see Fig.3.7). The maximal value of the single-line gain on the vibrational transition was observed for rotational number J = 12.

A comparison of results on gain measuring obtained through threshold characteristics (Fig.3.2) and the data on amplification (Figs.3.6 and 3.7) demonstrates that there is 1.5 - 2.0 times difference between the values of laser gain obtained by different methods. In case of the measurement of threshold characteristics we measured the real SSG, but in case of MOPA system we could have

measured saturated gain. There was no published information about saturation energy or intensity for FO CO laser system. To estimate saturation energy and intensity, theoretical calculations of FO CO laser amplifier characteristics were done.

3.3.3. Theoretical analysis of FO CO laser amplifier characteristics

Saturation parameters

By definition, SSG corresponds to amplification of laser radiation of such a low intensity that does not influence on the inversion dynamics. With a growth of incident radiation intensity the inversion will diminish. Generally, this decrease of gain is governed by time dependence of the amplified radiation intensity and vibration-vibration exchange dynamics. Two limiting situations can be distinguished: laser pulse is short in comparison with characteristic kinetic time; amplification proceeds in quasi-steady-state mode. In our experiments both limits are not realized. However, to give a general idea about an order of magnitude of gain saturation effects some information here is provided about so called saturation energy strictly applicable for short pulse amplification. Further, some results of calculations will be presented illustrating that simple mechanism of gain saturation described by a law $g=g_0(1+I/I_s)^{-1}$ is not applicable for FO CO laser.

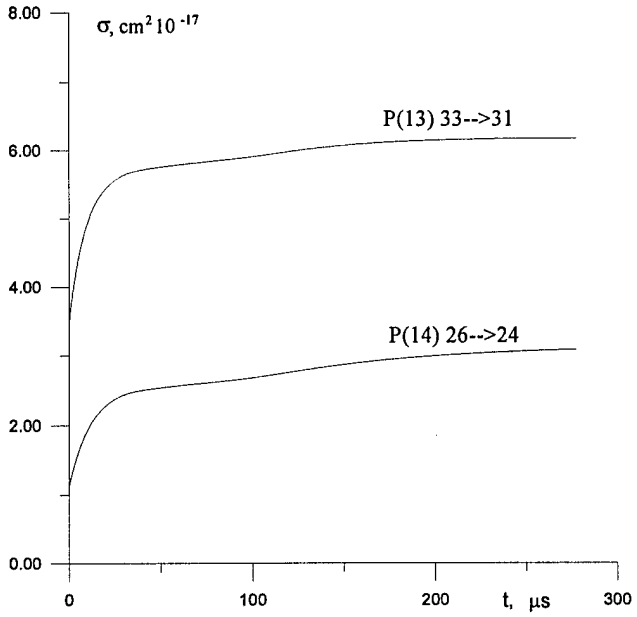

Fig.3.8. Time behavior of effective stimulated emission cross section σ for two ro-vibrational transitions. CO:N_2 = 1:9, gas density 0.12, T_0 = 100 K, SIE = 360 J/l Amagat

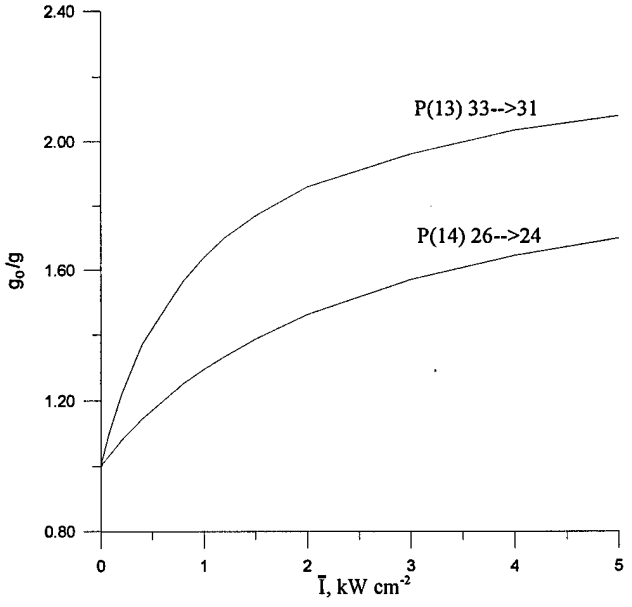

Fig.3.9. Dependence of g_0/g on average laser input intensity.

In the experiments, the net gain in the amplifier is small, and this permits us to apply approximation of the thin amplifying layer for the theoretical analysis. It means that spatial non-uniformity of the laser intensity and gain coefficient are neglected. The intensity is put equal to the injected from the MO radiation intensity varying in time. Numerically, the evolution of the gain is

found to be governed by discharge excitation and saturation caused by the incident radiation. The used kinetic model was the same as in [Ionin et al., 1999c], i. e. with a proper account of multi-quantum vibrational exchange. The values of g were calculated for several transitions by formula:

$$g = \frac{\int g(t)I(t)dt}{\int I(t)dt}$$

In the limit of the short pulse no collisional relaxation of population on the laser levels takes place. (It should be noticed that we mean under term collisional relaxation the processes controlling total population of the vibrational level assuming that the rotational relaxation is instantaneous.) Saturation of gain is a result of radiative stimulated transitions, and is characterized by the saturation energy $E_s=h\nu/\sigma_{vj}$. Table 3.1 demonstrates the dependence of this saturation energy on rotational number J for vibrational band 33→31 and gives value of saturation energy for P(14) 26→24 ro-vibrational transition. It should be noted that the stimulated emission cross section (SECS) for conditions of the experiment varies in time because of rising gas temperature of the active medium, as it is seen in Fig.3.8. The quantities were defined at the moment 120 μs after beginning of active medium excitation.

Table 3.1.

P(J) V+2→V	σ, cm^2 10^{-17}	E_s, mJ cm^{-2}	I_s, kW cm^{-2}	τ_k, μs
P(10) 33→31	8.48	0.31	0.709	0.87
P(13) 33→31	6.00	0.44	0.952	0.92
P(15) 33→31	4.20	0.625	1.39	0.9
P(18) 33→31	1.98	1.32	3.03	0.87
P(14) 26→24	2.5	1.18	2.9	0.81

SSG and saturation effects were studied theoretically for single-line FO CO laser radiation. The conditions were taken close to the experimental ones described above. The incident MO laser pulse started at 100 μs after the discharge initiation and had a triangle shape with the leading edge duration 20 μs and the tail 80 μs. Time interval corresponding to the time of MO laser radiation interaction with the laser amplifier is of the same order as the characteristic time of formation and free evolution of the energetic gain. Therefore, it is anticipated that the saturation effect is more complicated than it is predicted by the simple theory. Nevertheless, to show how far from traditional one is the process of gain saturation, the results of numerical simulations were plotted as

dependence of g_0/g on the average laser radiation intensity (see Fig.3.9). Here g_0 is the small signal gain. For traditional saturation mechanism in steady state conditions $g_0/g=1+I/I_s$. Evidently, slope of the curve in the low intensity limit gives the inverse of the saturation intensity. Results of calculations demonstrate that the actual gain saturation proceeds much slower than the traditional one. The saturation intensity defined from the zero-intensity limit strongly varies with vibrational and rotational numbers. Partially, this variation is associated with variation of the stimulated emission cross section and laser frequency. General expression for the saturation intensity has a form: $I_s= h\nu/\sigma_{v,j}\tau_k$, where τ_k is the characteristic inversion relaxation time. From mechanism of inversion formation in CO laser it follows that this characteristic time is not only function of gas mixture thermodynamic parameters, but depends also on the conditions of the excitation (discharge power, duration of pumping pulse). In afterglow conditions this characteristic time explicitly depends on time variable. Therefore, it is not surprising that looking at the Fig.3.9. one can see quite different saturation phenomenon than traditional one. To estimate the characteristic time introduced above, the effective time was calculated from an expression $\tau_k = h\nu/(\sigma_{v,j}I_s)\equiv E_s/I_s$, where I_s was taken in the limit of zero intensity (see **Table** 3.1). It is worth to note that the kinetic time constant is approximately the same for all rotational components of the 33→31 transition despite that the SECS varies several times in magnitude.

It should be noted, that the experiments on single-line amplification (see 3.3.2) were carried out, when master-oscillator pulse length $\tau_{out}>>\tau_k$. The intensity of input signal ~50-100 W/cm^2 was much lower than saturation intensity (Table 3.1). Therefore, Figs.3.4-3.7 represent SSG. Its value, smaller than one obtained from threshold lasing experiment (Fig.3.2), seems to be related to higher temperature of active medium in the second laser facility used as a laser amplifier in these experiments.

Relaxation time

Using developed theoretical model and experimental method based on double Q-switched mode of FB CO laser operation described and studied in [Ionin et al., 1999c, d] we performed a comparative analysis of measured data and data calculated by developed multiquantum exchange (MQE) and traditional single quantum exchange (SQE) models. The restoration time τ_{rest} of second Q-switched laser pulse energy with respect to the first's one was analyzed because it is very important time characteristic of the vibrational energy exchange process.

Taking into account the fact that in the experiments on measuring the dependencies of $R=Q_2/Q_1$ on τ_{1-2} ($Q_{1(2)}$ - the energy of the first (second) Q-switched laser pulse, τ_{1-2} - delay time between them) the maximal values of R for different ro-vibrational transitions were in the interval

0.8-0.9, we define the restoration time τ_{rest} as τ_{1-2} corresponded to the value of R=0.8 and called it as $\tau_{0.8}$. Experimentally measured values of $\tau_{0.8}$ for different ro-vibrational laser transitions and for fixed characteristics of active medium and laser radiation [Ionin et al., 1999c, d] were in the range of 3.6-6.3 μs. The values of $\tau_{0.8}$ measured experimentally and calculated using two theoretical models mentioned above are presented in Table 3.2.

Table 3.2. Restoration time $\tau_{0.8}$ for different FB CO laser transitions calculated by SQE and MQE models and measured experimentally (Time delay between the beginning of pump pulse and the first Q-switching of laser resonator τ_d=590 μs, laser mixture CO:N_2=1:1, initial gas temperature T=100 K, laser mixture density N=0.047Amagat).

Table 3.2.

Transition, V→V-1 P(J)	**SIE,** J/l.Amagat	$t_{0.8}$, μs SQE	MQE	Experiment
13→12 P(11)	250	2.30	5.80	6.3
13→12 P(11)	290	2.30	5.30	4.2
15→14 P(13)	330	1.70	5.45	4.0
15→14 P(13)	375	1.50	5.00	3.6
19→18 P(15)	330	1.45	5.80	5.5
20→19 P(14)	560	1.30	3.60	3.7

As one can see from the Table 3.2, the MQE model gives better agreement with the experimental data than the SQE model. A significant difference between values of $\tau_{0.8}$ calculated by two models is needed to be explained. After fast perturbation of vibrational population produced by the first Q-switched lasing, the population is restored according to the following equation $d(\Delta n_v)/dt \approx -\Delta n_v/\tau_{vv}$, where n_v is population of the vibrational level v, Δn_v is perturbation of the population, τ_{vv} is relaxation time due to the processes of VV-exchange responsible for the population of the vibrational level v. This relaxation time is defined as:

$$1/\tau_{vv} = \sum_{m\geq 1} \sum_{i\geq m} n_i \cdot (Q_{i-m,i}^{v+m,v} + Q_{i-m,i}^{v,v-m}),$$

where $Q_{i-m,i}^{v+m,v}$ is rate constants of m-quantum exchange.

The dependencies of τ_{vv}^{-1} on a number v of vibrational level (population of which was disturbed) calculated for experimental condition using SQE and MQE models are presented in

Fig.3.10. One can see that for v>8 the frequency τ_{vv}^{-1} calculated with MQE model (curve 1) is significantly lower than one calculated with SQE model (curve 2). And what is more, for v>30 the difference may be up to 5 times. In addition, in Fig.3.10 we presented the curve 3 that illustrates the fraction of single-quantum exchange processes in the value of τ_{vv}^{-1} calculated with MQE model. Finally, the difference between the curves 1 and 3 demonstrates the role of multi-quantum exchange processes, that appeared to be very significant.

Vibrational distribution functions (VDF) calculated with SQE and MQE models at the moment of time corresponding to τ_d=590 μs (in the same conditions as for Fig.3.10) are presented in Fig.3.11. The comparative analysis of the two curves in Fig.3.11 agrees with the conclusion made in [Konev et al., 1994] about a week sensitivity of stationary VDF to the choice of the model of vibrational energy exchange.

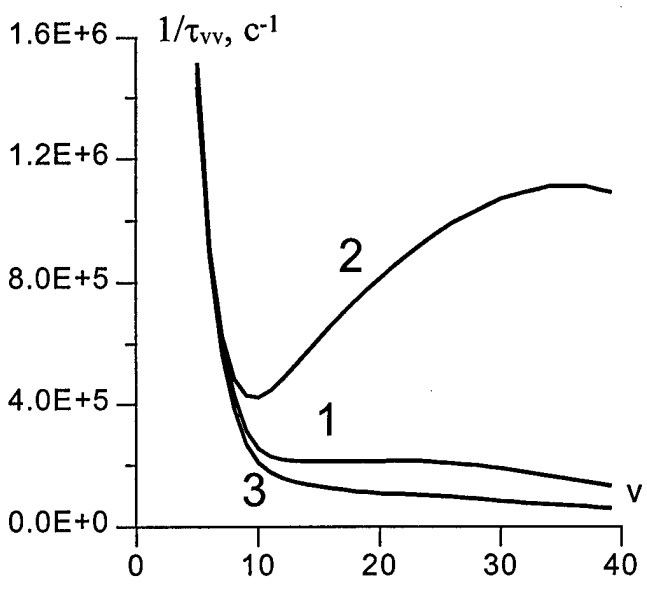

Fig.3.10. Dependencies of (τ_{vv}^{-1}) vs. vibrational quantum number v (corresponding to the level where population was perturbed) calculated with MQE (1) and SQE (2) models. Curve 3 illustrates the fraction of single-quantum exchange processes in the value of τ_{vv}^{-1} calculated with MQE model. CO:N_2=1:1, N=0.05 Amagat, T=100 K, SIE=290 J/l Amagat

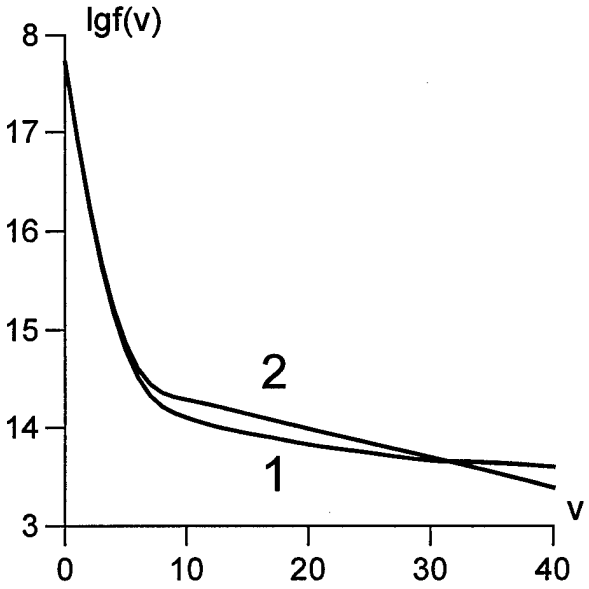

Fig.3.11. VDF calculated with MQE (1) and SQE (2) models in the same conditions as for the Fig.3.10.

Evolution of VDF in a gas excited by electrical discharge at low temperature is characterized by two stages. At the first stage, the accumulation of vibrationally excited molecules on lowest levels takes place. The duration of this stage is defined by specific input power per single molecule. After the reaching the critical amount of vibrational quanta per single molecule, further evolution of VDF is defined by VV-exchange processes between excited molecules. At this second stage, the "plateau" appears on the VDF. The plateau formation leads to appearing of partial inversion. The

duration of the plateau formation is defined by repeated VV-exchange processes and the rate of VDF evolution depends on effective exchange frequencies and the level of plateau. Approximately, characteristic time of VDF formation on fixed level is proportional to the square of the level number [Zhdanok et al., 1979], that is two orders higher than the time of vibrational quanta exchange for the molecules on the plateau. In our experiments this time equaled to hundreds microseconds. But measured restoration time $\tau_{0.8}$ is defined by the time of VV-exchange for the molecules on the plateau and one could expect its value in microsecond range. As we can conclude from our study, these assumptions are rather correct and correlate with both experimental data and theoretical calculations.

The parameter τ_{vv} is very important in laser kinetics, because it allows us to estimate the saturation intensity $I_S \approx h\nu/\sigma\tau_{vv}$ during selective lasing on both FB and FO transitions of CO molecule ($h\nu$ is radiation quantum on the transition frequency, σ - cross section of radiation induced transition). And the saturation intensity characterizes the non-linearity of active medium with respect to its interaction with laser radiation (see above). It makes sense to compare τ_{VV} obtained in above calculations with calculations obtained from theoretical simulations of saturation effect (Table 3.1) for the same experimental condition. The calculated values of τ_{VV} for vibrational levels V=26 and V=33 were 1 μs and 1.26 μs, respectively. One can see rather a good agreement with data from the Table 3.1 for τ_k, corresponding to the same vibrational levels.

3.3.4. Feasibility study of CO laser vibrational kinetics with FB CO MOPA system

Taking into account the experimental difficulties which appeared in our previous study of vibrational kinetics by double Q-switching in frequency selective FB CO laser (associated with too high threshold for lasing on transitions higher than $v \rightarrow v\text{-}1=20 \rightarrow 19$) [Ionin et al., 1999c, d], we started using modified experimental method to investigate the processes of vibrational levels population restoration after its fast perturbation. The developed optical scheme including two laser installations (MOPA system) is presented in Fig.3.12. The optical volume of power amplifier (PA) 1 was divided into two channels: the first one (2) was used as a free running frequency selective generator of low intensity laser radiation with laser pulse duration of ~2ms , the second one (3) was used as the active medium to be studied. The pumping of both channels was accomplished simultaneously and SIE in both channels was the same. The laser resonator in the first PA channel consisted of a diffraction grating 4 (150 grooves per cm, blazing angle 32^0 for λ=5.3 μm) and flat output mirror 5 (CaF_2 plate with interference coating, reflectivity ~94% for λ=5.3-6.0 μm). Master oscillator (MO) 6 was used as a generator of intense short frequency selective laser pulse with

duration of ~1μs. Its resonator consisted of diffraction grating 7 (150 grooves per cm, blazed at 29^0 for λ=5.8 μm), rotating flat totally reflecting Al mirror 8 (rotation speed up to 60000 revolutions per min) and flat CaF_2 output plate 9.

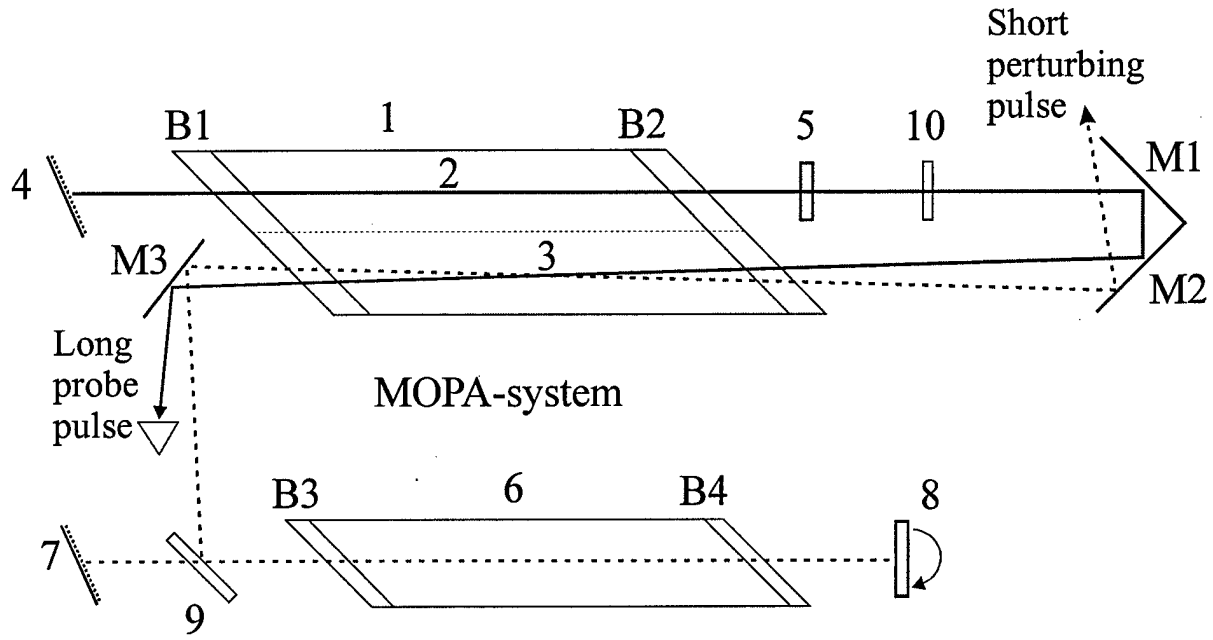

Fig.3.12. Modified optical scheme based on FB CO MOPA system for study CO laser vibrational kinetics. **1** - power amplifier, **2** - the first channel as probe long laser pulse generator, **3** - the second channel as active medium to be tested, **4&7** - diffraction gratings, **5** - output mirror of probe pulse laser resonator, **6** - master oscillator, **8** - rotating mirror, **9** - output coupler of short pulse laser generator, **10** - amplitude filter, **B1-B4** - Brewster windows, **M1-M3** - totally reflecting flat mirrors.

Single-line long laser pulse from the first channel of PA was attenuated by filter 10 and directed into the second channel of PA as week probe signal to test the temporal behavior of the gain (and, respectively, population inversion) on selected transition. Short laser pulse from MO was also directed into second channel of PA and supposed to disturb the populations on vibrational levels corresponded to transition selected in MO laser (ro-vibrational transitions selected in MO and in the first channel of PA were the same). Time synchronization of long laser pulse from PA and short laser pulse from MO was accomplished as follows: ~20 μs time interval on time profile of long probe laser pulse was chosen in such a way that its intensity was quasi-stationary, and the short disturbing laser pulse was delayed to enter the active medium of the second channel of PA in this time interval (see Fig.3.13).

As a result, we supposed to observe fast decrease of probe laser pulse intensity immediately after the short disturbing of population inversion in the second channel of PA by laser pulse from MO with its following growth up to the initial quasi-stationary value. From this time dependencies of gain (and, respectively, population inversion on selected transition) we planned to obtain direct

kinetic information for comparing the theory and experiments on laser transitions higher than 20→19.

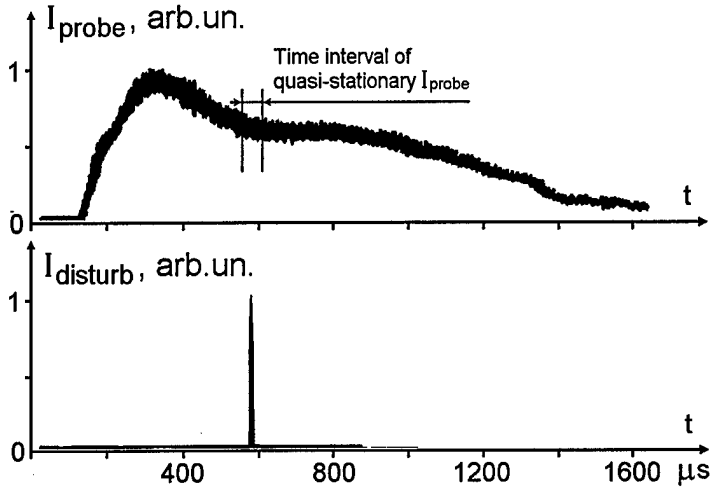

Fig.3.13. Experimentally obtained time behaviors of probe and perturbing laser pulse intensities.

Unfortunately, using this optical scheme we couldn't obtain any reliable experimental data by the moment. As we understand, two factors prevented us from positive results:

1) The short laser pulse energy in our experiments was too low to disturb significantly the population inversion on selected transition, i.e. it was not enough to decrease gain on selected transition at least ~10-20% down for reliable measuring.

2) If the probe laser pulse time profile was detected with high temporal resolution, a deep (~20%) high frequency modulation of its intensity took place (it was due to mode beating in conditions of near threshold operation). This beating does not allow us to separate the gain changes connected with population inversion perturbation, if any (Fig.3.14).

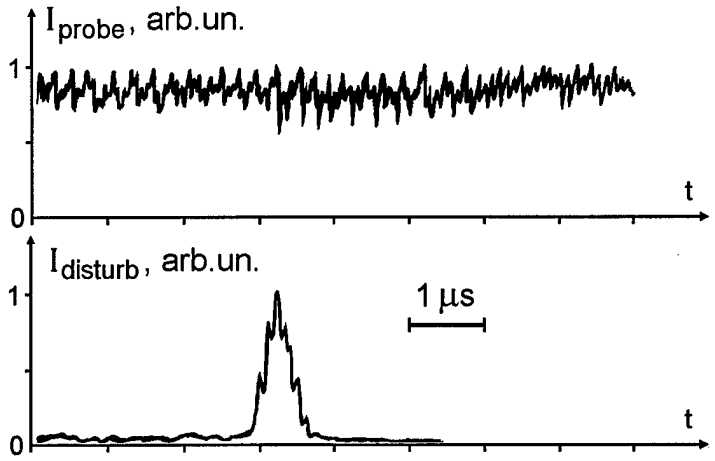

Fig.3.14. Experimentally obtained time behaviors of probe and perturbing laser pulse intensities at high temporal resolution.

For these reasons we propose to change experimental technique for study the vibrational kinetics in the following way:

short intensive disturbing population inversion (and, respectively, the gain in the active medium) should be produced by single pulse Q-switching of the resonator of frequency selective CO laser. As a probe laser one should use single-line CW CO laser with its output intensity stabilized as high as possible.

3.4. Conclusions

FO CO laser MOPA system was launched for the first time, multiline SSG coming up to 1.2 10^{-3} cm^{-1}. Time behavior of multiline gain was demonstrated with FO CO laser MOPA system. The maximal multiline gain was obtained, when MO radiation pulse started 100-200 μs later than pump pulse of the amplifier.

Single-line SSG was measured by threshold lasing method and with MOPA system. The maximum value of SSG came up to ~1.5 10^{-3} cm^{-1}, that is comparable with previous measurements. Taking into consideration the data from Part 2, we would claim, that SSG lies within ~1.0-2.0 10^{-3} cm^{-1} for FO CO laser active medium.

Theoretical analysis of saturation effect and relaxation time was accomplished, saturation energy and intensity being calculated. A comparison of the theoretical data with the experimental results indicates, that we observed non-saturated amplification and did measure SSG. A calculation of relaxation time for some vibrational transitions accomplished by two different ways resulted in approximately the same values.

Preliminary experiments on using MOPA system for studying CO laser kinetics were carried out indicating necessity of using low power cw master oscillator in the experiments.

4. Modeling of RF discharge plasma

4.1. Introduction

RF discharge is widely used for gas laser pumping. A general tendency in last years is to replace fast flow gas lasers with power up to 5 kW to lasers excited by RF discharge in slab configuration. Slab geometry allows for effective thermal diffusion cooling of discharge gap due to narrow spacing. Electrodes used to be cooled by a liquid. A loop with blowers and refrigerators for this liquid are much simpler (in particular, with low noise) than a respective loop in fast-flow lasers. In comparison with a transverse dc discharge, RF discharge possesses better stability, and electrode layers occupy smaller fraction of discharge gap. These are major advantages that cause a rapid development of RF discharge technique in applications to high-power gas lasers manufacturing. In particular, CO lasers with slab geometry were developed in several groups (Zhao et al, 1991; von Bulov et al, 1990) with RF discharge exciting laser medium in the resonator and in subsonic part of the supersonic nozzle, respectively.

Concerning discharge physics, there are some features common to different active media including CO_2, CO lasers. However, discharge properties are more or less predictable and can be reasonably explained only for CO_2 laser. We are not aware of any theoretical modeling of RF discharge in CO laser. Generally, structure of discharge is expected to be in both lasers quite similar. Nevertheless, there are no simple relations between characteristics of electrode layers and plasma bulk in different gas mixtures. Moreover, there are indications on much stronger influence of vibrational excitation on plasma characteristics in CO laser than in CO_2 laser (Grigor'yan et al, 1992).

At present, there exist detailed models of RF pumped CO_2 lasers predicting laser characteristics in a good agreement with experiment, in respect to as discharge structure, as laser parameters (Ilukhin et al, 1995). To develop a similar model for RF pumped CO laser it would be convenient to break the problem on two sub-problems. The first concerns detailed kinetic modeling of processes in CO plasma. It is important to account for coupling between electron and vibrational kinetics. In the detailed kinetic model existing now, parameters of discharge were put equal to measured in the experiments assuming them independent of vibrational excitation. This is true, when the electron kinetics is controlled by e-beam ionization. For non self-sustained discharge when ionization produced by plasma electrons or in collisions of excited molecules becomes about 0.1 from the e-beam ionization, immediately an instability develops. Therefore, in a stable mode of operation the positive feedback between plasma excitation and ionization is negligible. For RF discharge this positive feedback is expected to be important, maybe dominant, in a regular regime.

The second sub-problem concerns description of a real discharge structure. As a rule, electrode layers varying in time can not be neglected introducing a big deal into an impedance of the discharge and hence the power dissipated in the bulk. Besides, these layers occupy some fraction of the discharge gap that can not be found analytically. Therefore, one-dimensional model should be developed to describe time evolution of discharge properties.

4.2. Modification of the kinetic model

To develop a full kinetic model it is convenient to form four groups of processes:

1. V-V exchange, V-T relaxation and interaction of molecules with electrons involving change of vibrational state;
2. Electron scattering from molecules and atoms, heating of electrons by electric field;
3. Kinetics of electronically excited molecules and ions;
4. Thermal balance in plasma.

The first group of processes can be described in terms of a Vibrational Distribution Function (VDF), dynamics of which is controlled by a source (excitation by electrons), a sink (V-T relaxation) and V-V exchange processes. In a steady state the source term is equilibrated by the sink. Usually V-V exchange proceeds much faster than V-T relaxation. This is a key condition for realization of the self-pump mechanism in CO laser.

The second group of processes is described in terms of the Electron Energy Distribution Function (EEDF). The rate of relaxation of the EEDF is controlled by electron-molecule collisions, and is of the order 10^8 - 10^{10} s^{-1}. Therefore, for typical RF discharge conditions it may compete only with RF frequency. The relaxation length of the EEDF for gas mixtures typical for CO laser at pressure tens-hundreds of Torr is of the order of a few or ten micrometers. It means that the EEDF sees only local parameters of plasma. Hence the homogeneous form of the electron Boltzmann equation (BE) is applicable. Time dependence of the EEDF shape may be important for some conditions, but a common approximation widely used in theory is based on solving steady state BE for instantaneous parameters. In dependence on the ratio of the RF field frequency and the EEDF relaxation frequency, a parameter governing electron kinetics is the reduced electric field strength E/N or E_{eff}/N, where $E_{eff} = E\nu_m[2(\omega^2+\nu_m^2)]^{-1/2}$. Here E is electric field strength amplitude, N is gas density, ω is RF frequency and ν_m is electron momentum relaxation frequency.

The third group includes processes with characteristic times longer, as a rule, than the EEDF relaxation time. Generally, the spectrum of characteristic frequencies for this group is rather broad extending from kHz up to MHz. The specific feature of these processes is that they are very sensitive to detailed shapes of the VDF and EEDF. However, an influence that they exert on

formation of both distribution functions is negligible. From the other hand, they play an important role in a balance of charged particles, in particular, they control the electron number density. It means that these processes affect very strongly on operation point of the discharge. It should be noted that information about reactions and their rates for this group is very limited.

The fourth group of processes includes gas heating in the discharge and cooling by thermal diffusion to the walls (electrodes). Generally, processes of energy release into gas heating for conditions of CO laser are quite complicated and include V-T relaxation, anharmonic energy defect dissipation in V-V processes, so called direct heating by electrons (energy dissipation in elastic collisions and through excitation of molecular rotation), some heating in processes of electronic state relaxation and chemical reactions. Fortunately, in the steady state heating by the sum of all processes is equal to Joule heating by electric current. Estimations demonstrate that diffusion of excited molecules can be neglected for typical conditions of the RF pumped CO laser. It means that non-local effects in gas heating also can be ignored. Strictly speaking, in the operating laser part of energy is removed from the volume with the laser radiation. This fraction characterized by laser efficiency can be calculated in the laser model.

Our model, described earlier in the reports (for example, (Ionin et al, 1997)), includes three of groups reviewed above. The only missing group of processes (it can be ignored for stable e-beam controlled discharge) is the third group. Therefore, in the present report these additional processes are described. Some effects produced by this extension of the model are described for conditions typical for RF pumped room-temperature CO lasers: gas mixture $CO:N_2:He=1:2:7$ at pressure 100 Torr, gas temperature T=300 K. In illustrating calculations the simplest electric circuit was assumed consisting of dc voltage supply connected to the discharge with spacing 1 cm and electrode area 1 cm^2 through the ballast resistor 3 kΩ.

To analyze balance of plasma density, it is necessary to take into account various ways in which vibrational excitation may influence on processes of ionization. These are direct and indirect ones. To the direct influence on the ionization, one can ascribe the process of associative ionization in collisions of partners one of which is CO or N_2 molecule on high vibrational level. The existence of processes of this sort is proved by experiments with optical pumping of CO molecules by resonant radiation (Flament et al, 1992). Implicitly, the vibrational excitation may influence on the ionization rate through the deformation of the (EEDF). It is known that at the fixed E/N value due to the growth of the vibrational energy a high-energy tail of the EEDF appears. The second potentially important process is the energy transfer process (V-E exchange) from vibrations to electronically excited levels. Electronic metastables produced in such a process may participate further in

collisions with other excited molecules resulting in ionization. Moreover, some new reactive channels became open when one of the collision partners is vibrationally excited. To calculate correctly plasma density all these processes should be included in the model.

In Fig. **4.1** an energy diagram is presented where electronically excited molecules and ions are included. The long lived electronic levels for N_2 and CO are shown. They play a particular role in possible ionization mechanisms.

Molecular energy terms are presented in Figs. **4.2** and **4.3** for CO and N_2, respectively. It is seen that higher energy terms are characterized by a minimum at longer inter-nuclear distance than the ground state. It means that cross sections for electron impact excitation of excited terms from the ground one should grow with the vibrational number. A problem of calculation these cross sections was considered earlier in (Alexandrov et al, 1985), where the dependence of cross section for excitation of the state $N_2(A^3\Sigma_u^+)$ on the vibrational number was found. A similar procedure for excitation of the state $CO(I^1\Sigma^-)$ was realized by us. The resulting cross sections as a function of electron energy for some selected numbers of vibrational levels are shown in Fig. **4.4**. The effective excitation threshold lowered with vibrational number, and maximum cross section for excited molecules about three times higher than for molecules in ground state. For the non-equilibrium VDF the effect of increasing electron cross section should be stronger.

A list of plasma chemical processes included additionally in our model is presented in **Table 4.1**. It should be noted that, while composing this list, some processes were neglected because of a small input in the kinetics. An example is formation of negative ion O^- in a process $CO+e \rightarrow C+O^-$ followed by a fast electron detachment in collisions with CO molecules. Only one type of positive ions was left in the model, $C_2O_2^+$ because of very fast transformation of all other ions (He^+, He_2^+, N_2^+ and so on) into this one. Most important for us are the processes of ionization associated with collisions of vibrationally or electronically excited molecules. Because of scarce information on dynamics of electronically excited molecules, any suggestions about additional mechanisms involving excited molecules are subject to validation by the experiment.

In this respect, the situation with studies on gas discharge stability in nitrogen may serve as an encouraging sample. Special experiments with control on discharge plasma homogeneity have proved a big role of vibrationally excited molecules in a mechanism of discharge current contraction (Napartovich et al, 1993). Formulation of a complete kinetic model including mechanisms of associative ionization in collisions of electronically and/or vibrationally excited molecules results in a satisfactory description of experimental data on discharge dynamics for quite different conditions. In particular, instability time for self-sustained discharge at pressure 50 Torr (Berdyshev et al, 1988)

and e-beam sustained discharge at pressure 1 bar (Berdyshev et al, 1989) was calculated with a high accuracy. Experimental data on discharge contraction in gas mixtures of CO laser (Golovin et al, 1986) demonstrated that contraction time is almost independent of CO concentration in the mixture CO:N_2. It may be considered as an indication on similarity of ionization processes in N_2 and CO. However, adding CO to nitrogen results in re-distribution of the vibrational energy from N_2 to CO. Then, the ionization processes introduced in (Berdyshev et al, 1988) lose the value. We suppose that similar processes exist, which involve CO vibrationally and electronically excited molecules. In the mechanism successfully describing instability of gas discharge in nitrogen, the key role played molecules in electronic state $N_2(a'^1\Sigma_u)$. It is necessary to define an electronic state of CO, which might play a similar role. The metastable state $CO(a^3\Pi)$ is inappropriate because of low energy. One can see from Fig. **4.2** that in the range of energy around 7 eV several closely spaced terms take place. Authors of (Grigor'yan et al, 1992) proposed that molecules in the state $CO(I^1\Sigma^-)$ may play a key role in associative ionization processes. We believe that this is a good idea. Therefore, CO molecules in this state were introduced in the model. Reactions for them include, additionally with respect to (Grigor'yan et al, 1992), $CO(I^1\Sigma^-)$ formation in collisions of two vibrationally excited CO molecules with the total energy higher than 9.45 eV. This condition is realized for molecules on the levels higher than 19.

Table 4.1

CO, N_2, He, CO(v), N_2(v), He*(19.8)^x, He^+(24.6), $CO(a^3\Pi)$(6), CO*(7), $CO(I^1\Sigma^-)$(9.45), CO^+(14.1), $C_2O_2^+$(13.1), N_2(A)(7.5), N_2^+(15.6), CO_2, C

1	**Reaction**	Rate, cm^3/s	Reference	Remark
1	$CO + e \leftrightarrow CO(v) + e$	From BE	Aleksandrov et al, 1986	$\sigma_v(v) = \sum_{v=1}^{10} v\sigma_{0v}(u)$
2	$N_2 + e \leftrightarrow N_2(v) + e$	From BE	Aleksandrov et al, 1986	$\sigma_v(v) = \sum_{v=1}^{8} v\sigma_{0v}(u)$
3	$CO(v) + e \leftrightarrow CO(I^1\Sigma^-) + e$	From BE	Aleksandrov et al, 1985	Like for $N_2(A^3\Sigma^+_u)$
4	$CO + e \leftrightarrow CO(a^3\Pi) + e$	From BE	Land, 1978	
5	$CO + e \leftrightarrow CO^* + e$	From BE		CO* is sum of high energy electronic levels
6	$CO + e \leftrightarrow CO^+ + e + e$	From BE	Land, 1978	
7	$CO(I^1\Sigma^-) + e \rightarrow CO^+ + e + e$	From BE		estimated

8	$CO(a^3\Pi) + e \rightarrow CO^+ + e + e$	From BE		estimated
9	$CO^* + e \rightarrow CO^+ + e + e$	From BE		estimated
10	$C_2O_2^+ + e \rightarrow CO + CO$	From BE	Grigor'yan et al, 1997	
11	$N_2 + e \leftrightarrow N_2(A) + e$	From BE		$N_2(A)$ is sum of all electronic levels
12	$N_2 + e \rightarrow N_2^+ + e + e$	From BE	Phelps et al, 1985	
13	$N_2(A) + e \rightarrow N_2^+ + e + e$	From BE		estimated
14	$He + e \leftrightarrow He^* + e$	From BE		He* is sum of high energy electronic levels
15	$He + e \leftrightarrow He^+ + e + å$	From BE	Dyatko et al, 1984	
16	$CO(I^1\Sigma^-) + CO(v>14) \rightarrow C_2O_2^+ + e$	$2K_{22}$	Grigor'yan et al, 1992	$14<v<40$
17	$CO(I^1\Sigma^-) + CO(I^1\Sigma^-) \rightarrow C_2O_2^+ + e$	$5\ 10^{-12}$	Berdyshev et al, 1988	Like for N_2
18	$CO(I^1\Sigma^-) + CO(a^3\Pi) \rightarrow C_2O_2^+ + e$	$6\ 10^{-12}$	Berdyshev et al, 1988	Like for N_2
19	$CO + He^* \rightarrow CO^+ + He + e$	$1\ 10^{-10}$	Zhiglinskii, 1994	
20	$N_2 + He^* \rightarrow N_2^+ + He + e$	$1\ 10^{-10}$	Zhiglinskii, 1994	
21	$CO(v>19) + CO(v>19) \rightarrow CO(I^1\Sigma^-) + CO$	$2.5\ 10^{-15}$	Berdyshev et al, 1988	$19<v<40$ Like for N_2
22	$CO(I^1\Sigma^-) + CO \rightarrow CO_2 + C$	K_{22}	Grigor'yan et al, 1992	$K_{22}=3\ 10^{-12}$
23	$CO(a^3\Pi) + CO \rightarrow CO_2 + C$	$1.4\ 10^{-12}$	Trubacheev, 1977	
24	$CO(a^3\Pi) + CO \rightarrow CO(v) + CO(v)$	$0.8\ 10^{-10}$	Ionikh et al, 1986	
25	$CO^* + CO \rightarrow CO_2 + C$	$1.4\ 10^{-11}$		estimated
26	$N_2(A) + CO \rightarrow N_2 + CO$	$2\ 10^{-12}$		estimated

[x]Numbers in parenthesis is the energy of the state in eV.

To illustrate effects predicted by the formulated block of the full kinetic model some simplified calculations were made. In these calculations, the VDF was prescribed in accordance with an analytical theory (Gordiets et al, 1986) at fixed gas temperature 300 K. It was assumed that

a piece of plasma with dimensions 1x1x1 cm^3 was connected through the ballast resistor 3 kΩ with a power supply providing constant voltage 1.4 kV. Then the system of kinetic equations was solved numerically in parallel with the BE for electrons. In such a way, the influence of vibrational excitation on the EEDF and electronic states populations was accounted for approximately.

Calculated evolution of voltage drop on the plasma, electric current and power dissipated in the gas together with the average electron energy is shown in Fig. **4.5** in dependence on time. Up to the moment 250 μs, processes involving high vibrationally excited (v>14 and v>19) CO molecules were ignored in the model by putting concentrations of them equal to zero. Molecules on the levels >14 are involved in an associative ionization reaction #16 in the **Table 4.1.** Molecules on the levels higher than 19 participate in a reaction of V-E transfer #21 in the **Table 4.1**. At the moment 250 μs populations of the above mentioned vibrational states were introduced in a stepwise manner. This results in a fast (for about 10 μs) growth of electric current with correspondent decrease of the voltage drop. The established electron energy is about 1 eV. Change of concentrations of a number of species in plasma induced by this procedure is illustrated in Fig. **4.6.**

Table 4.2

Value, reaction	Without high vibrational levels	With high vibrational levels
E/N, 10^{-16} Vcm^2	3.47	1.55
n_e, cm^{-3}	$1.11\ 10^{11}$	$6.47\ 10^{11}$
<U>, eV	1.721	1.077
V_e, cm/s	$5.58\ 10^6$	$2.92\ 10^6$
P_{disch}, W/cm^3	110	149
η_V^{CO}, %	26.6	52.0
$\eta_V^{N_2}$, %	61.8	55.0
$CO(v) + e \leftrightarrow CO(I^1\Sigma^-) + e$	$6.49\ 10^{-12}$	$1.17\ 10^{-14}$
$CO + e \leftrightarrow CO(a^3\Pi) + e$	$3.45\ 10^{-10}$	$2.46\ 10^{-12}$
$CO + e \leftrightarrow CO^* + e$	$8.65\ 10^{-11}$	$2.23\ 10^{-13}$
$CO + e \leftrightarrow CO^+ + e + e$	$9.08\ 10^{-14}$	$4.97\ 10^{-19}$
$CO(I^1\Sigma^-) + e \rightarrow CO^+ + e + e$	$2.81\ 10^{-11}$	$1.43\ 10^{-13}$
$CO(a^3\Pi) + e \rightarrow CO^+ + e + e$	$9.67\ 10^{-12}$	$1.18\ 10^{-14}$
$CO^* + e \rightarrow CO^+ + e + e$	$1.44\ 10^{-11}$	$3.07\ 10^{-14}$
$C_2O_2^+ + e \rightarrow CO + CO$	$3.69\ 10^{-7}$	$4.33\ 10^{-7}$
$N_2 + e \leftrightarrow N_2(A) + e$	$8.00\ 10^{-11}$	$1.38\ 10^{-13}$
$N_2 + e \rightarrow N_2^+ + e + e$	$1.93\ 10^{-14}$	$2.14\ 10^{-20}$

$He + e \leftrightarrow He^* + e$	$1.54\ 10^{-16}$	$1.07\ 10^{-23}$
$He + e \leftrightarrow He^+ + e + å$	$5.69\ 10^{-19}$	$2.33\ 10^{-28}$

It is interesting that the number of molecules $CO(I^1\Sigma^-)$ grows while other electronic levels are strongly depopulated. This is explained by existence of the processes of energy transfer from vibration to the electronic state. As a result, electron number density also increases about an order of magnitude, despite that the ionization by electron impact became negligible because of low voltage and electron energy. In agreement with the experiment (Grigor'yan et al, 1992), where remarkable increase of discharge voltage was observed as a result of laser oscillations suppression, our model demonstrated strong dependence of sustaining voltage on populations of high vibrational levels. This effect is illustrated also by **Table 4.2** where some quantities are compared calculated before and after the step shown in Fig. **4.5**. Diminishing of the average electron energy causes strong re-distribution of excitation energy flow from electrons between vibrations of CO and N_2. The rate of processes with a high-energy threshold (including step-wise ionization and excitation of molecules) drops from two to seven orders of magnitude. It means that collisional processes involving vibrationally excited molecules became dominant in ionization of gas.

4.3. About modeling of RF discharge structure

RF discharges in typical for gas lasers conditions (gas pressure around 100 Torr, electrode spacing 1-3 mm, field frequency in 100 MHz range) have essentially non-uniform profiles for laser gain and gas temperature resulting from non-uniform plasma density and electric field distributions. In our group, there is a numerical code for simulations of RF discharge in gas mixtures of CO_2 laser. An example of typical distributions of parameters of RF discharge is given by Figs. **4.7** and **4.8**. Electric field and electron number density profiles are characterized by existence of electrode layers with a positive charge and strong electric field (see Fig. **4.7**). Usually, gas temperature growth exerts a negative influence on laser gain. Therefore, most optimum conditions for gain may realize not far from the border between bulk of plasma and electrode layers. The result is formation of non-monotonous gain profile similar to shown in Fig. **4.8** where the gas temperature profile is displayed, too. The numerical code developed for description of RF pumped CO_2 laser can be modified in respect to vibrational kinetics and plasma chemistry to reflect specific features of CO laser. This may be the task for further progress of modeling RF pumped CO laser. However, one may anticipate that simple combining of full kinetic model with the sub-routine calculating time-space evolution of discharge structure will result in enormous increase of computational time. Therefore, an approach based on some preliminary analysis and simplifications looks more promising for achieving the final goal.

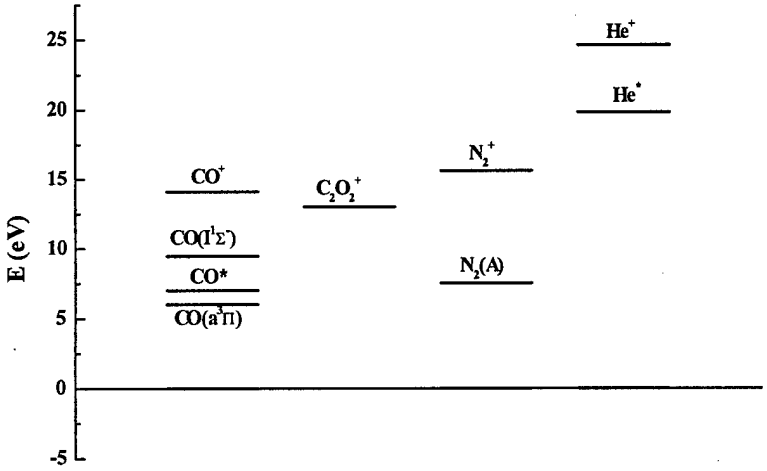

Fig. 4.1. Energy diagram for species included in the model

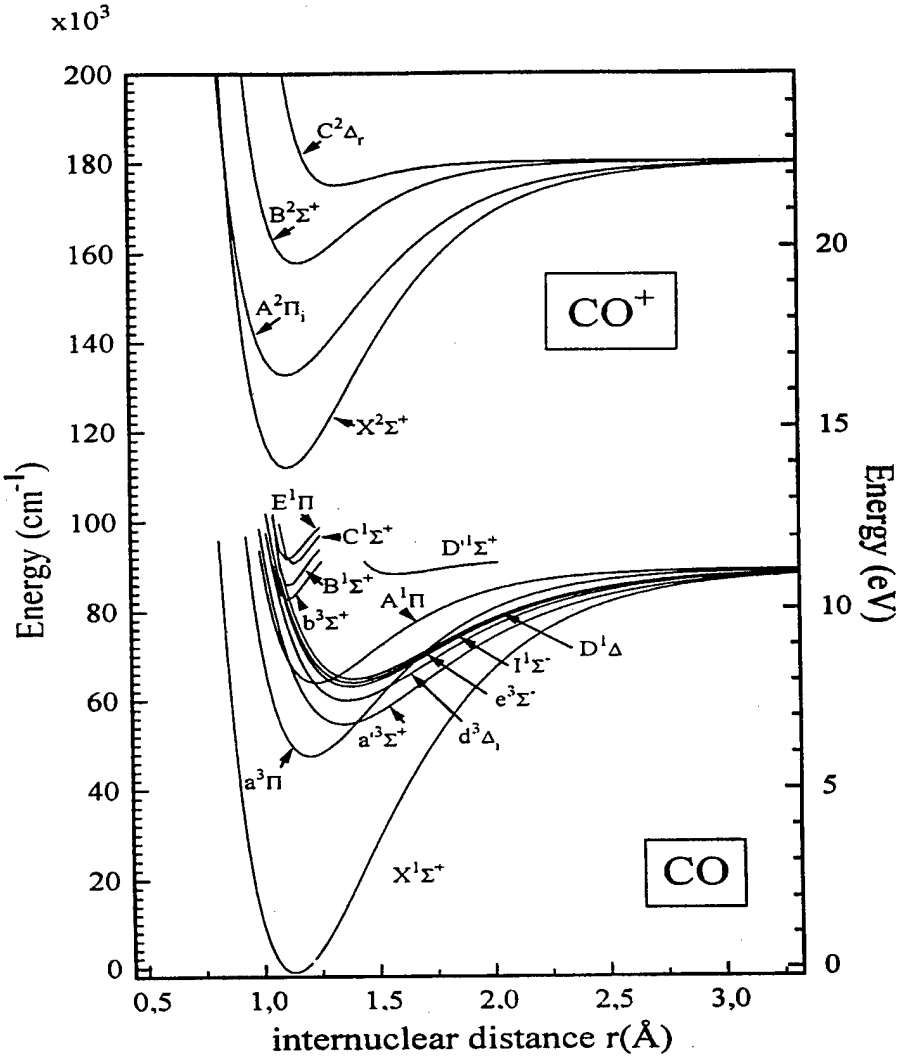

Fig. 4.2. Molecular terms for CO molecule

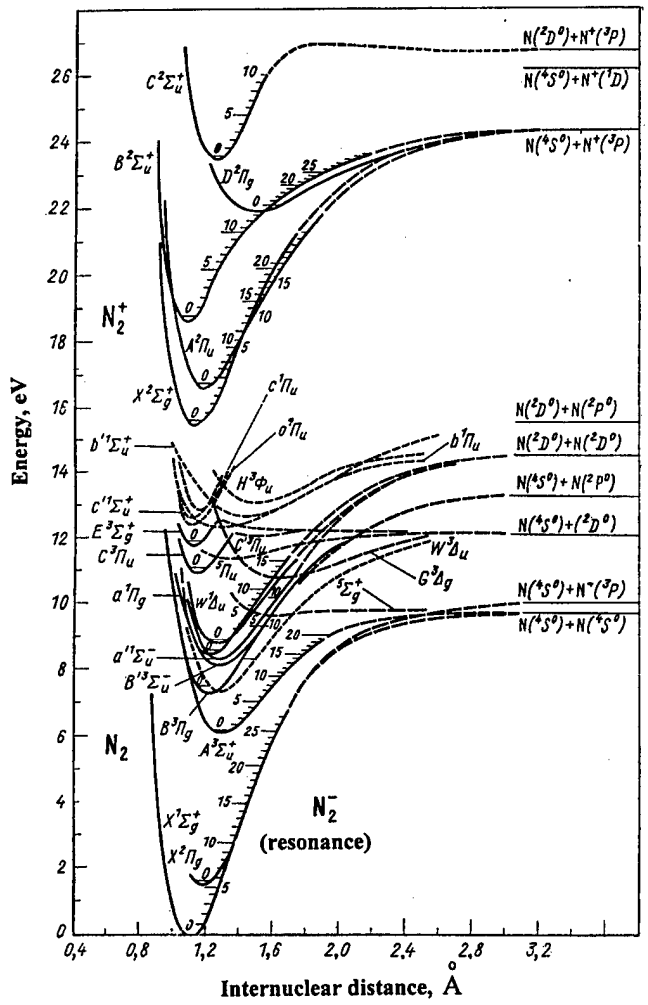

Fig. 4.3. Molecular terms for N_2 molecule

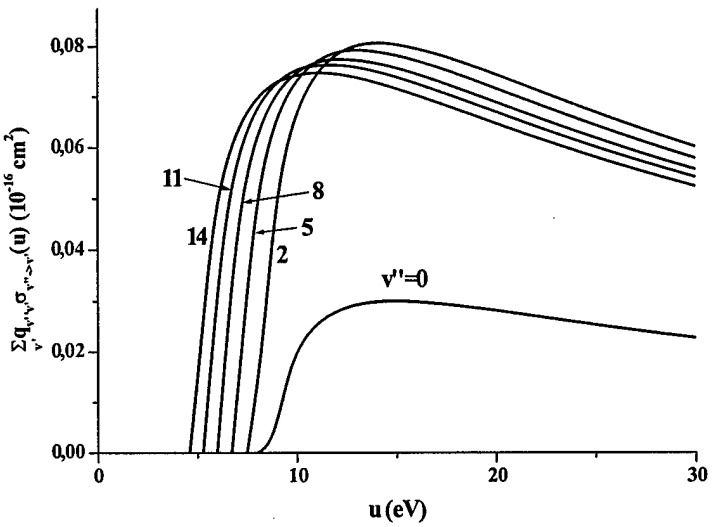

Fig. 4.4. Cross sections for electron impact excitation of $CO(I^1\Sigma^-)$ from selected vibrational levels of ground state; v′ and v″ are vibrational level numbers for upper and lower terms, respectively

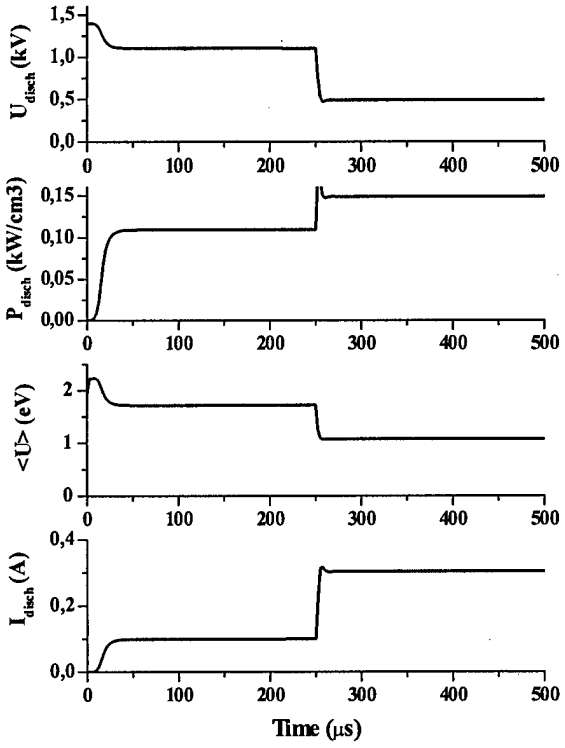

Fig. 4.5. Time evolution of discharge characteristics calculated with the simplified model

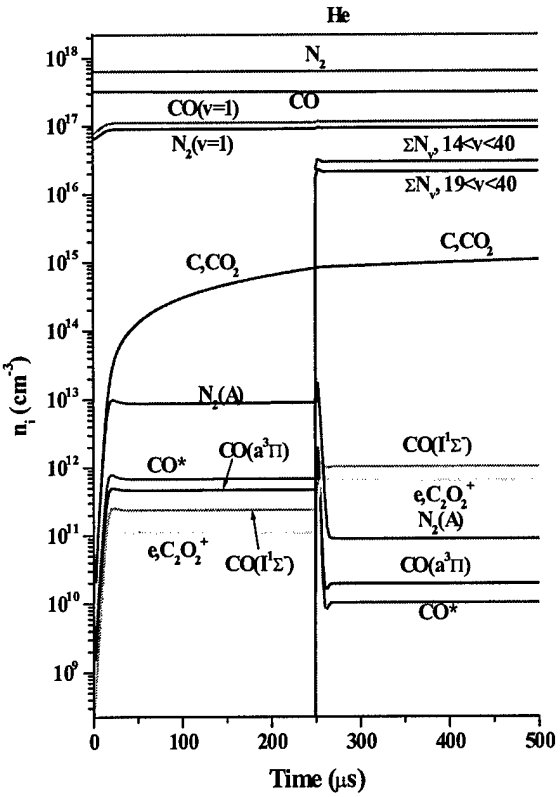

Fig. 4.6. Time evolution of concentrations of different species in plasma calculated with the simplified model

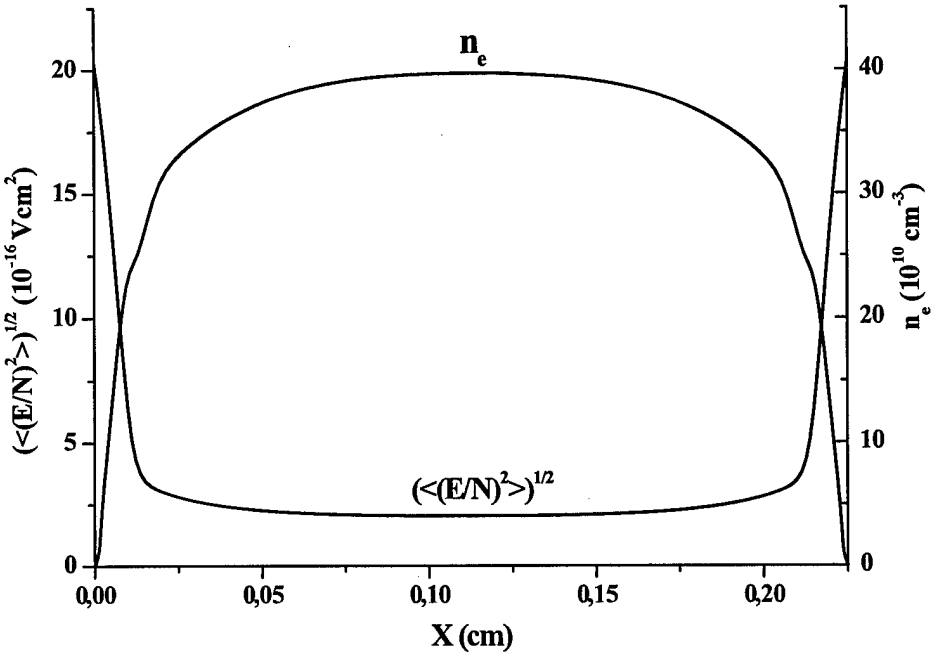

Fig. 4.7. Calculated spatial profiles of electron number density and RMS value of E/N averaged over RF cycle. P = 100 Torr, T_w = 293 K, CO_2:N_2:He=1:1:5, $W_{discharge}$ = 147 W/cm^3, d = 0.225 cm, f = 190 MHz.

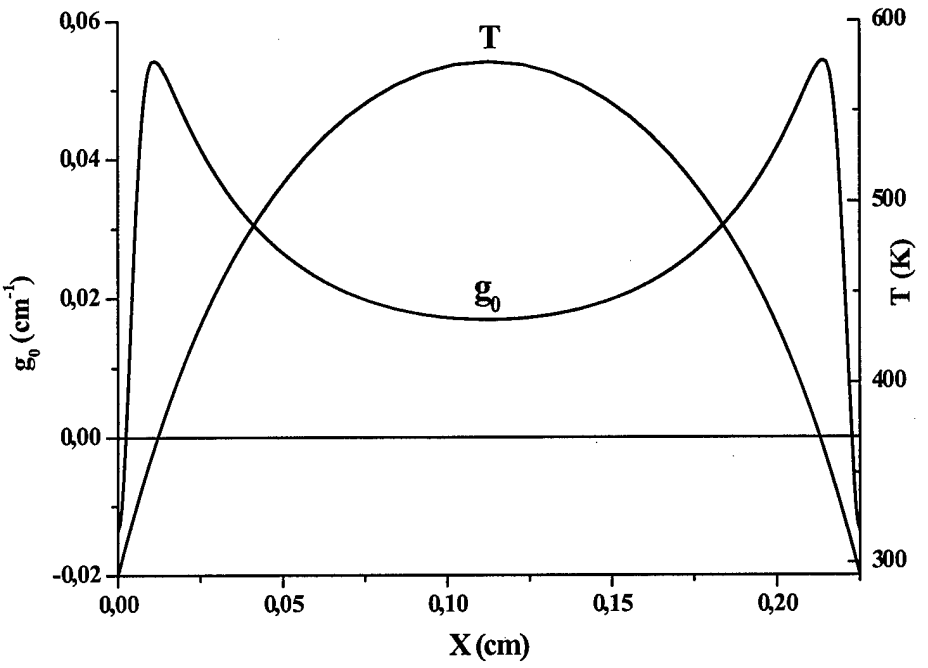

Fig. 4.8. Calculated spatial profiles of small signal gain and gas temperature. P = 100 Torr, T_w = 293 K, CO_2:N_2:He=1:1:5, $W_{discharge}$ = 147 W/cm^3, d = 0.225 cm, f = 190 MHz.

4.4. Conclusions

The problem of theoretical description of RF pumped CO laser operating both in fundamental and overtone bands was never solved satisfactorily. To develop the relevant model it is necessary to describe space-time structure of the discharge in a self-consistent manner together with vibrational kinetics. Such an approach was realized in modeling RF pumped CO_2 lasers. Modifying the model of this kind to include processes specific for CO laser, one meets some difficulties. The first is much more complicated vibrational kinetics for typical conditions of CO laser, in particular for operation in the overtone band. The second is strong coupling between kinetic of electrons, electronically excited and vibrationally excited molecules. In this respect, there are some experimental indications to this coupling and no reliable data about dominant processes. Here we report about a version of kinetic model that possesses properties similar to observed in the experiments with glow discharges. From the other side, we report that we have at hand the numerical code describing satisfactorily the RF discharge in mixtures of CO_2 laser. This numerical

code may be taken as a basis for further modifications to extend description onto mixtures and conditions typical for CO laser.

Conclusions

Output characteristics of FO CO laser using different combinations of dielectric mirrors from AFRL were studied with paying much more attention to the laser spectral characteristics. The effect of alternation of vibrational band intensities related to two independent lasing cascades over vibrational levels of CO molecule was observed experimentally. Examination of optical characteristics of mirrors serving in the laser for a long time demonstrated that some changes in them took place which may influence on laser output and selectivity of mirrors.

Single-line FO CO lasing was obtained on more than 400 spectral lines corresponding to overtone transitions from 13→11 up to 38→36 within spectral range of 2.7-4.2 μm, maximum efficiency being 0.6%. Multiquantum approach was applied for theoretical description of FO CO laser, better agreement being demonstrated between theoretical and experimental results for laser output versus vibrational quantum number. Taking into consideration multiline FO CO lasing within 2.5-4.1 μm, one can claim FO CO laser to have very broad spectrum lying within 2.5-4.2 μm.

FO CO laser MOPA system consisted of two laser facilities was launched. Single-line SSG was experimentally measured by using MOPA system and threshold lasing, SSG being (1.0-2.0) 10^{-3} cm^{-1}. Saturation effect and relaxation time of vibrational population were theoretically calculated.

Existing kinetic model was extended to include plasma chemical processes controlling ionization degree in a self-sustained discharge. Strong influence of vibrational excitation degree on ionization-recombination balance in plasma for typical for RF discharge conditions was demonstrated.

High efficiency and high specific output energy obtained in the experiments places the FO CO laser amongst other high-power lasers such as CO_2 laser, FB CO laser, HF(DF) laser, its spectrum region covering that of HF and DF lasers and the number of spectral lines, many of which coincide with absorption lines of many substances, being much higher. FO CO laser can be considered as a new efficient source of high-power IR radiation.

Experimental and theoretical study of FO CO laser and MOPA system demonstrated, that there are some scientific problems to be considered in further research.

New mechanism of interaction of highly excited CO molecules with N_2 molecules needs to be involved in the theoretical model and experimentally analyzed by study of influence of nitrogen, helium and argon on spectral characteristics of FO CO laser operating on very high (38→36) vibrational transitions.

SSG and saturation parameters are needed to be calculated and measured for a manifold of highly excited vibrational levels. This information, together with data on time restoration of inversion population for highly excited (V>20) vibrational levels obtained by double Q-switching procedure and/or by using MOPA system amplifying short FB CO laser pulse, is quite necessary for further developing FO CO laser theoretical model.

Further efforts are needed to verify the model describing RF discharge plasma characteristics both experimentally and theoretically. Unfortunately, information that can be found in literature about RF discharge characteristics in CO laser mixtures, in particular operating within the FO band, is very scarce. Therefore, the next step in the work program should contain experimental measurements of the RF discharge characteristics and theoretical simulations capable to predict plasma instabilities and so called photo-voltaic effect in the discharge. To complete the model of the RF pumped CO laser, the existing subroutines for simulation of plasma kinetics and space-time evolution of discharge structure should be combined. This is a non-trivial problem requiring a detailed analysis of most important processes in plasma.

References

Alexandrov N. L., Kochetov I. V., Napartovich A. P., 1985, Teplofiz. Vys. Temp., v. 23, 849 (in Russian)

Alexandrov N. L., Kochetov I. V., Napartovich A. P., 1986, Khimiya. Vys. Energ., v. 20, 291 (in Russian)

Bachem E., A. Dax, T. Fink et al, 1993, Appl. Phys., B57, 185

Basov N.G., V.A. Danilychev, A.A. Ionin et al, 1978, Kvantovaya Electronika, 5, 1833 (in Russian)

Basov N.G., V.S. Kazakevich, I.B. Kovsh, 1980, Kvantovaya Electronika, 7, 1966 (in Russian)

Basov N.G., A.A. Ionin, I.B. Kovsh, 1985, Infrared Physics, 25, 47

Basov N., G.Hager, A.Ionin, A.Kotkov et al., 1999a, Proc. Int. Conf. LASERS'98, 7-11 Dec, 1998, Tucson, AZ, USA, Ed. by V.Corcoran & T.Goldman, STS Press, McLean, VA, USA p.481

Basov N., G.Hager, A.Ionin, A.Kotkov et al., 1999b, "Multiline and single-line pulsed first-overtone CO laser frequency tuned within spectral range of 2.5-4.2 μm", Preprint #15 of P.N.Lebedev Physics Institute, Moscow pp.1-23

Basov N., G.Hager, A.Ionin, A.Kotkov et al., 1999c, Opt.Comm., v.171, p.107

Belykh A. D., V. A. Gurashvili, I. V. Kochetov, A. K. Kurnosov, A. P. Napartovich, V. M. Putilin, N. G. Turkin, 1995, Quantum Electronics 25 315.

Berdyshev A. V., Kochetov I. V., Napartovich A. P., 1988, Fizika Plazmy, v. 14, 742 (in Russian)

Berdyshev A. V., Golovin A. S., Gurashvili V. A. et al, 1989, Fizika Plazmy, v. 15, 335 (in Russian)

Bergman R.C., Rich J.W., 1977, Appl.Phys.Lett. 31, p. 597.

Billing G. D., 1986, Vibration-vibration and vibration-translation energy transfer, including multiquantum transitions in atom-diatom and diatom-diatom collisions, in: Non Equilibrium Vibrational Kinetics, M. Capitelli, Ed. Berlin, Germany: Springer Verlag, pp. 85-112.

Bronshtein I., Semendyaev K., 1986, "Mathematics handbook", Nauka, Moscow, pp.441-466 (in Russian)

von Bulov H., Zeyfang E., 1990, Proc. SPIE v. 1397, 499.

Demjanov A. V., I. V. Kochetov, A. P. Napartovich et al, 1979, Teplofizika Vysokikh Temperatur, 18, 918, (in Russian)

Dyatko N. A., Kochetov I. V., Napartovich A. P., Taran M. D., 1984, Teplofiz. Vys. Temp., v. 22, 1048 (in Russian)

Flament C., George T., Meister K.A. et al., 1992, Chemical Physics, v. 163, 241

Gordiets B. F., Zhdanok C. A., 1986, in "Nonequlibrum vibrational Kinetics", edited by M. Capitelli

Golovin A. S., Gurashvili V. A., Kochetov I. V., et al, 1986, Teplofiz. Vys. Temp., v. 24, 852 (in Russian)

Grigor'yan G. M., Ionikh Y. Z., Kochetov I. V. et al, 1992, J. Phys. D: Appl. Phys., v. 25, 1064.

Grigor'yan G. M., Ionikh Y., 1997, Teplofiz. Vys. Temp., v. 35, 702 (in Russian)

Gromoll-Bohle M., W. Bohle and W. Urban, 1989, Opt. Comm., 69, 409

Guelachvili G., D. de Villeneuve, R. Farrenq, W. Urban, J. Verges, 1983, J. Mol. Spectr. 98, 64.

Ilukhin B. I., Udalov Yu. B., Kochetov I. V., Ochkin V. N., Heeman -Ilieva M. B., Peters P. J. M., Witteman W. J., 1996, Applied Physics B, v. 62, 113.

Ionikh Y. Z., Kuranov A. L., Lobanov A. N. et al, 1986, Opt. Spectrosc., v.60, 444 (in Russian)

Ionin A. A., H. Kobsa, K. Kleine, 1996a, Proc. SPIE 3092, 422

Ionin A. A., Yu. M. Klimachev, Yu. B. Konev, A. K. Kurnosov, I. V. Kochetov, D. V. Sinitsyn, 1996b, Proc. SPIE 3092, 301

Ionin A., Napartovich A., Kotkov A., Kurnosov A. et al, 1997a, "Experimental and Theoretical Study of First Overtone Carbon Monoxide Laser Physics", Scientific Report of the Lebedev Institute on Contract SPC-97-4014 with EOARD.

Ionin A. A., Yu. M. Klimachev, H. Kobsa, D. V. Sinitsyn, 1997b, Quantum Electronics 27, 744.

Ionin A., A.Kotkov, A.Kurnosov, A.Napartovich et al, 1998a, Proc. Int. Conf. LASERS'97, Dec 1997, New Orleans, LA, USA, STS Press, McLean, VA, p.92

Ionin A.A., A.A. Kotkov, A.K. Kurnosov, A.P. Napartovich et al, 1998b, Opt. Comm., 155, pp. 197-205

Ionin A.A., A.A. Kotkov, A.K. Kurnosov, A.P. Napartovich, L.Seleznev et al., 1998c, "Experimental and Theoretical Search of Conditions for Maximum Efficiency and for Frequency Tunability of IR Overtone CO Laser", Scientific Report of Lebedev Institute on Contract SPC-97-4066 with EOARD

Ionin A. A., Yu. M. Klimachev, H. Kobsa, D. V. Sinitsyn, 1998d, Proc. SPIE 3343, 1032.

Ionin A. A., Yu. M. Klimachev, Yu. B. Konev, A. K. Kurnosov, I. V. Kochetov, D. V. Sinitsyn, 1998e, "Double pulse lasing in single-line Q-switched CO laser', in: Proc. Int. Conf. on LASERS' 97, V. J. Corcoran and T. A. Goldman, Eds. McLean, VA: STS Press, pp. 88-91.

Ionin A., A. Kotkov, A. Kurnosov, A. Napartovich, L. Seleznev et al, 1999a, "Frequency tuning of IR first-overtone CO laser radiation by diffraction grating and frequency selective output couplers", Scientific Report of Lebedev Institute on Contract SPC-98-4076 with EOARD

Ionin A.A., A.A. Kotkov, A.K. Kurnosov, A.P. Napartovich, L.Seleznev et al, 1999b, Opt. Comm., 160, pp. 255-260

Ionin A., A. Kotkov, A. Kurnosov, A. Napartovich, L. Seleznev et al, 1999c, "Study of vibrational exchange and determination of V-V exchange rate constants on high levels of CO molecule", Scientific Report of Lebedev Physics Institute on Contract SPC-98-4088 with EOARD

Ionin A. A., Yu. M. Klimachev, Yu. B. Konev et al., 1999d, Multi-quantum vibrational exchange of highly excited CO molecules, Preprint of P. N. Lebedev Physics Institute, Moscow, (to be published).

Konev Yu.B., Kochetov I.V., Kurnosov A.K. et al., 1994, J.Phys.D:Appl.Phys., v.27, p.2054

Land J. E., 1978, J. Appl. Phys. v. 49, 5716.

McCord J. E., A. A. Ionin, S. P. Phipps, P. G. Crowell, A. I. Lampson, J. K. McIver, G. D. Hager, 2000, Frequency tunable optically pumped carbon monoxide laser, in: Int. Conf. AHPLA '99, Osaka, Japan, 1-5 Nov, 1999, Technical Program, p. 25, paper 3889-94; Proc. SPIE 3889.

Murtz M., B. Frech, P. Palm, R. Lotze, and W. Urban, 1998, Opt. Lett. 23, 58.

Napartovich A. P., Akishev Y. S., 1993, Proceedings of XXI ICPIG, v. 3, p. 207, Bochum.

Phelps A. V., Pitchford L. C., 1985, JILA information center, report #26.

Suchkov A. F., Yu. N. Shebeko, 1979, Kvantovaya Elektronika, 6, 360 (in Russian)

Trubacheev E. A., 1977, Trudi FIAN AN SSSR, Gazovie laseri i ikh primenenie, pod red. N. N. Soboleva, v. 102 (in Russian)

Yardley J. T., 1970, J. Mol. Spectr. 35, 314

Zhao H., Baker H. J., Hall D. R., 1991, Appl. Phys. Lett., v. 59, 1281.

Zhiglinskii A. G., 1994, Spravochnik konstant elementarnikh protsessov s uchastiem atomov, ionov, electronov, fotonov, Sankt-Peterburg (in Russian)